International Journal of Fatigue 186 (2024) 108383

Contents lists available at ScienceDirect

International Journal of Fatigue

journal homepage: www.elsevier.com/locate/ijfatigue

On fatigue behavior of short cracks subjected to compressive underloads

Kimmo Kärkkäinen [a,*], Joona Vaara [c,b], Miikka Väntänen [d], Mari Åman [a], Tero Frondelius [c,a,b]

[a] Materials and Mechanical Engineering, University of Oulu, Pentti Kaiteran katu 1, 90014, Finland
[b] Faculty of Built Environment, Tampere University, Korkeakoulunkatu 7, 33720, Finland
[c] R&D and Engineering, Wärtsilä, P.O. Box 244, 65101, Vaasa, Finland
[d] Global Boiler Works Oy, Lumijoentie 8, 90400 Oulu, Finland

ARTICLE INFO

Keywords:
Variable amplitude loading
Crack closure
Fracture mechanics
Fatigue strength
Numerical modeling

ABSTRACT

This work explores the effects of underloads on physically short fatigue cracks propagating under near-threshold zero–tension loading in various constraint conditions. A finite element model is employed to model the transient behavior of plasticity-induced crack closure and residual stress, from which propagation behavior can be inferred. The expected behavior of acceleration after an underload is mostly descriptive of the plane stress results, but in axisymmetric and plane strain conditions a post-underload deceleration is predicted with single or scarce underloads. Frequently repeated underloads, however, are found to reduce fatigue strength in all cases considered. Short cracks prove especially vulnerable to underload acceleration when initiated at notch-like defects. Three independent physical mechanisms are recognized, namely, the removal of load history, compressive notch plasticity, and Bauschinger effect, a combination of which explains the underload results. Additionally, tentative guidance for fatigue design in finite and infinite life underload applications is provided.

1. Introduction

In engineering applications, components under fatigue rarely see pure constant amplitude loading. In addition, over- and underloads have been shown to have a significant influence on subsequent crack propagation. It is therefore very important to also consider the effects of variable amplitude loads to maintain an understanding of the components' remaining fatigue life. While the actual loading conditions may be quite stochastic and difficult to assess in a quantitative manner, it is most helpful to thoroughly understand the effects of single over- and underloads. The variable amplitude loading sequence of a components service life is, to a varying degree, an arbitrary series of the aforementioned loading irregularities.

Plasticity-induced crack closure, discovered by Elber in 1970 [1], is an intrinsic mechanism reducing crack driving force. In Mode I tensile loading, even with small nominal load amplitudes, a plastic zone is formed in front of the crack tip. This tensile plastic strain is not fully reversed during load reversal, and thus these residual plastic strains persist. Once the crack propagates into this residual plastic strain field, a geometric incompatibility arises between the newly formed regions of the crack flanks, denoted as a plastic wake, and the crack will come in contact sooner in unloading, and can remain in contact for a considerable portion of the load cycle even with stress ratios above zero [2]. This concept, later expanded to cover also other types of crack surface contact, such as oxide and roughness-induced crack closure, has then been successfully used to predict the effects of stress ratio, over- and underloads, for example.

It is well known that different loading irregularities cause transient propagation behavior in fatigue [3–31]. A single overload has been shown to most often reduce crack propagation rate for a relatively large number of subsequent loading cycles, or even halt crack growth altogether. An underload on the other hand, by which a compressive overload is referred as in present work, has been shown to have the opposite, but usually more subdued, effect. It is commonly reported that a fatigue crack subjected to a single underload experiences a transient acceleration of crack growth, with the crack growth rate quickly recovering to pre-underload levels with subsequent propagation.

The most common physical explanations given in literature for the observed over- and underload effects are residual stresses and crack closure, a brief overview of which is presented in Table 1. Both effects are intimately linked to crack tip plasticity and cannot fully be separated, see Fig. 1.

The effect of overloads on fatigue crack propagation behavior is comprehensively covered in literature, and a fairly robust agreement has been established. Underloads, on the other hand, have received noticeably less attention, even though they are more dangerous of the

* Corresponding author.
E-mail address: kimmo.karkkainen@oulu.fi (K. Kärkkäinen).

https://doi.org/10.1016/j.ijfatigue.2024.108383
Received 26 February 2024; Received in revised form 9 May 2024; Accepted 10 May 2024
Available online 14 May 2024

Table 1
A brief overview of the two main mechanisms behind the observed over- and underload effects according to the authors' understanding of current literature.

	Residual stress	Crack closure
Overload	An overload stretches the material in the crack tip plastic zone, thus creating a field of more intense compressive residual stress in front of the crack tip. By superposition with the nominal loading, this residual stress lowers the effective stress ratio and reduces the local stress in the crack tip once the crack advances into the overload plastic zone, hindering crack propagation.	Immediately after an overload, all existing crack closure is removed due to crack tip blunting, causing a sharp increase in crack propagation rate. Once the crack propagates into the overload plastic zone, the compressive residual stress relaxes and transforms into a higher-than-baseline residual displacement. This causes plasticity-induced crack closure to strengthen, hindering crack propagation through a reduction of the effective, open-crack portion of following load cycles.
Underload	An underload causes reversed plasticity in the plastic wake and crack tip plastic zone, reducing the level of compressive residual stress both at the current crack tip position and in front of the crack tip. This in turn immediately raises the effective stress ratio and local stress, accelerating propagation. The base-level compressive residual stress would recover in the very next tensile load, but as the new plastic zone extends in an oblique angle (approx. 45°), the recovery of the superposition stress at the crack tip only takes place after a small distance of subsequent crack propagation.	The reversed plasticity caused by an underload can likewise remove existing crack closure by compressing the existing crack wake, accelerating propagation initially. Material also in front of the crack tip is compressed when compared to the baseline state. This reduction in plastic strain results in a lesser residual displacement of the crack flanks once the crack traverses into the underload-affected zone. In correspondence, weaker plasticity-induced closure and elevated propagation rate prevail until the crack tip is once again under a steady-state baseline plastic wake.

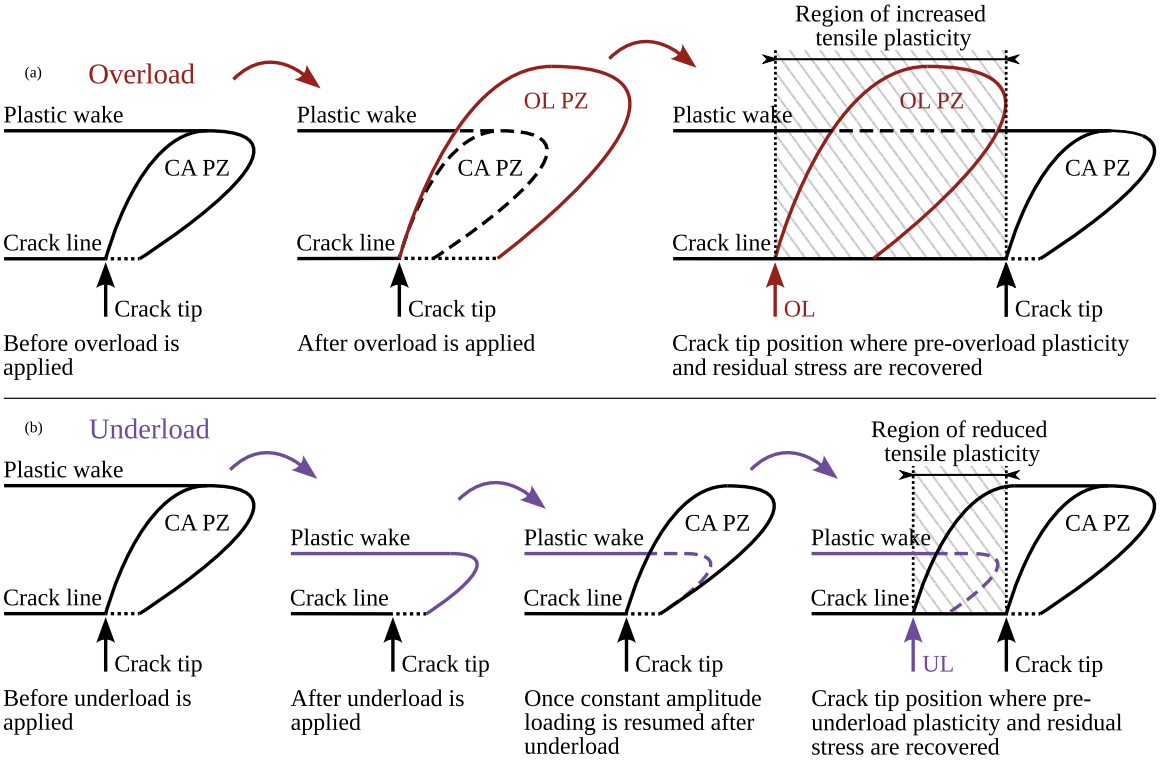

Fig. 1. Schematic visualization of crack wake plasticity when a single (a) overload or (b) underload is applied, according to the authors' understanding of current literature. The figure contains the following acronyms: constant amplitude (CA), plastic zone (PZ), overload (OL), and underload (UL).

two in terms of fatigue life. Underloads are even commonly disregarded in fatigue predictions, as negative loads are thought not to affect the fatigue process [10]; a misconception that may lead to unconservative estimates. Most experimental and numerical data available in the literature, considering the effect of underloads, are from through-plate long cracks, and reports considering short and/or radial 3D cracks are very sparse. Long, through-plate cracks do not fully represent the critical cracks in most engineering components, which is why a surge of investigations into small, 3D cracks has recently began to take place [32–34].

Consideration of over- and underload behavior in short cracks is a crucial aspect in terms of fatigue life, and much work is needed in this area. The short crack regime in near-threshold loading conditions is where the most decisive effects are experienced, making the crack either arrest or propagate. This paper attempts to unravel how physically short cracks behave when subjected to underloads through considerations of plasticity-induced crack closure and near-tip residual stresses. The present article is structured followingly. First, an overview of the relevant literature is presented. Next, the details of the chosen finite element modeling strategy are provided. Then, results obtained from the finite element analyses are presented, based on which preliminary guidance towards accounting for underloads in fatigue design could be provided. In an earlier work investigating the effect of over- and underloads to plasticity-induced crack closure in internal cracks [35], an unexpected finding was made, where crack retardation was consistently predicted in underload scenarios. As this behavior contrasts with the general literature consensus of crack acceleration after an underload, a detailed analysis of the physical mechanisms behind this phenomenon is provided in the discussion. This helps to enhance the understanding of underload effects. As a by-product, the present work deepens the

conception of plasticity-induced crack closure, carrying insight not only limited to the underload case, or short cracks.

2. Literature review

Both experimental [3,6–8,10–14,16,18,19,21–24,28,30,31] and numerical [6,9,15,17,21,22,25,26,30,31] methods have been used to study the overload [3,6–9,12–19,21,23–25,28,30] and underload [8–11,15–18,21,22,26,30,31] phenomena in fatigue. While most works report retardation after an overload [3,6–9,12,13,15,17–19,21,23–25,28] and acceleration after an underload [8,9,15,16,18,21,22,26,31], accounts of post-overload acceleration [14,16] and post-underload retardation [10,11,17] also exist. The underlying mechanisms for the transient crack growth behavior are crack tip tensile plasticity and crack tip blunting for overloads, and crack wake reversed plasticity for underloads. Crack closure [6,7,10,17,22,24,26,31] and residual stresses [23,24,31] are the concepts most used to explain and quantify the effects on crack growth rate. The significant parameters of the problem are specimen geometry (plane strain [8,10,11,16] or plane stress [7,14,22,26,31] dominated), material (especially cyclic plastic properties and hardening behavior [16,17,26]), over- and underload magnitude [21,23,30,31], as well as base loading stress ratio [16,22,26,30,31] and magnitude [8,21,31]. A qualitative consensus regarding long crack effects has been reached in most situations with overloads, and at least in plane stress dominated cracks under zero–tension or tension–tension base loading with underloads. Questions remain on the short crack response [5,8,12,13], the relative influence of crack closure and residual stress [16,17,23,24], as well as the discrepancies between observations and prediction models [6,11].

2.1. Differences between over- and underloads

There exists a fundamental difference between over- and underload plasticity, where the effect of reversed yielding near the crack tip associated with an underload is quickly erased with subsequent loading and crack advance, while an overload increases the size of the monotonic plastic zone, yielding a longer lasting effect (see Fig. 1). This is an unambiguous explanation for the difference in duration of the over- and underload effect [17,21,26,30]. While an overload is known to cause blunting of the crack tip, the reverse, crack tip sharpening, could be thought to occur with an underload, as mentioned by Salvati et al. [22]; however, they highlighted that empirical evidence by Fleck [36] suggests the opposite, that blunting could be observed in both cases. It could be postulated that the mechanism responsible for the apparent crack tip blunting following an underload would be compressive yielding of the existing crack flank plastic wake, enhanced by the Bauschinger effect.

2.2. Effect of constraint conditions

Plasticity-induced crack closure behaves very differently in plane stress and plane strain conditions [34,37,38], which is thought to play a role in the over- and underload effects. Dexter et al. [6] found the crack growth rates at constant amplitude loading to be dependent on the average closure through the thickness, while after an overload a better correlation was obtained considering only the surface closure levels. McEvily et al. [7] also found that plane stress closure was the dominant factor in overload crack growth transients; electro-discharge-machining off the plane stress surfaces after the overload was applied lead to a nearly instant recovery of the crack growth rate. This suggests a difference between the plane stress and plane strain overload response, and that the overload retardation effect is mostly controlled by plane stress closure in plate-like specimens.

2.3. Effect of stress ratio and baseline closure levels

Many authors have reported weaker underload effects with negative base loading stress ratios [16,22,26]. This behavior has been recognized to depend on the baseline closure levels [26], meaning that the underload effect would be enhanced by, for example, an overload preceding the underload [14,26]. Furthermore, in an overload–underload or underload–overload sequence the latter load spike has been recognized to determine the prevailing effect [23].

2.4. Crack closure versus residual stresses

There is an ongoing debate into whether the over- and underload effects are dominated by crack closure or residual stress. Sunder et al. [23] argued that the transient growth rates had nothing to do with crack closure, but rather near-tip residual stresses, which is conceivable at high stress ratios. Furthermore, Silva [16] as well as Ellyin & Ozah [17] both saw plasticity-induced crack closure more as a consequence of residual compressive stresses than a cause to the crack growth behavior. However, a study by Salvati et al. [24] attempted to separate the residual stress and crack closure mechanisms affecting overload behavior. They compared two different stress ratios of base loading, $R = 0.1$ and $R = 0.7$ in order to eliminate the contribution of crack closure in the latter. They concluded that while the residual stress mechanism is active in the entire R range, its effect is relatively short-lived, and that plasticity-induced closure has a dominant effect at all but the highest stress ratios. They also stated that with both stress ratios the influence of residual stress would be practically identical, which allowed for the superposition of the two mechanisms' contributions across the R range. However, the superposition may not be valid as it could be argued that, especially with metals exhibiting strong Bauschinger effect, the reversed plasticity following an overload could occur at base loading minima with low stress ratios, reducing the compressive residual stresses.

2.5. Tensile residual stresses

Many works report tensile residual stresses ahead of the crack tip after the application of an underload [16,17,22,31]; however, it is questionable whether a sustained tensile residual stress can exist near the crack tip once base loading is continued. The present authors would argue that the tensile residual stress effect should exist as more of a reduction of the base-line compressive residual stress, which should still induce crack acceleration. In terms of residual stress considerations with overloads, for instance, an intuitive presumption would be that the strongest compressive residual stresses would manifest at the crack tip immediately at the overload position. This would lead to difficulties in explaining the delayed retardation effect of the overload by compressive residual stresses. However, the most intense compressive residual stress should be experienced at that crack tip position in which the current crack tip plasticity, combined with plasticity of the former overload plastic zone, is at a maximum. Thus, much like the delayed effect of plasticity-induced crack closure after an overload, the residual stress effect is also intrinsically delayed. A similar effect can be conceived also with an underload, as the pre-underload compressive residual stress should not be recovered immediately at the next constant amplitude tensile loading, but only once the crack tip reaches the height of the new plastic zone (see Fig. 1(b)).

2.6. Post-underload retardation

Ellyin & Ozah [17] investigated plasticity-induced crack closure in single over- and underload situations with a 3D finite element model. They found that a single overload produced strengthening of plasticity-induced closure. With a single underload they found deviating behavior compared to the literature consensus, reporting an initial loss of closure

followed by closure levels stronger than those of constant amplitude loading, especially in the plane strain region. Correspondingly, some experimental analyses considering plane strain dominated geometries, corner cracks [10] and thick SEN-specimens [11], report retardation after underloads. The latter reference concluded that mechanisms other than plasticity-induced crack closure would be needed as the available prediction models accounting for said mechanism failed to predict the observed effect.

2.7. Fatigue limit and short cracks

Some experimental analyses consider overload interactions of short cracks [12,13]. These works conclude that the retardation effect following an overload is similar, if not strengthened with short cracks. Suresh et al. [5], however, have stated the opposite, that short cracks would not experience the retardation/acceleration effects to the same degree as long cracks. In the underload case Suresh et al.'s argument is supported by the above-reported dependence of the underload effect on the strength of pre-existing crack closure [26]; closure levels are generally lower with shorter cracks. Pompetzki et al. [8] noted a difference in the overload response between short and long cracks and argued that the initial acceleration associated with overloads is of primary importance for short cracks. They also discovered that both over- and underloads allow for subsequent load cycles below fatigue limit to extend damage. This implies a substantial reduction of fatigue limit if either loading irregularity is periodically applied. Short crack arrest commonly observed in near-threshold loading should therefore be inhibited if the loading contains over- and/or underloads. Underloads have also been reported to be able to resume the growth of non-propagating cracks [39]. Additionally, even larger pre-strain cycles have been shown to reduce fatigue life and scatter [40], indicating a bypassing of the initiation phase. In summary, both over- and underloads seem more detrimental when applied in the initiation/short crack phase than in the long crack regime, but not necessarily because of meaningfully different crack closure or residual stress effects, but because of the difference in criticality of crack extension.

3. Modeling methodology

The chosen modeling strategy for plasticity-induced crack closure, bearing resemblance to earlier works [34,35], is described in this section. The numerical simulations are carried out using the commercial finite element software ABAQUS/Standard. Numerical analysis methods, such as the finite element method, are great tools for conducting parametric studies considering crack propagation [2,37,41]. Numerical analysis allows for obtaining data difficult or impossible to obtain from traditional experiments, with a fraction of the cost. Obtaining accurate empirical data of such a small-scale phenomenon is exceedingly difficult, and while numerical data must be validated empirically, it can provide us with helpful information [2]. To obtain reliable results, the state-of-the-art numerical analysis has well-defined recommendations for crack growth scheme and element sizes, among others, which are discussed in more detail in this section.

3.1. Specimen geometry

Two different specimen geometries are used to investigate plasticity-induced crack closure; a rotationally symmetric cylindrical specimen with an internal spherical cavity and a plate-like specimen with a circular hole. The elastic stress concentration factors of the defects are $K_t = 3.0$ and $K_t = 2.0\overline{45}$, respectively, for the Poisson's ratio of $\nu = 0.3$ used in this study [42,43]. Both geometries are derived from the same 2D mesh by utilizing different sets of boundary conditions. The modeled geometry is a 2D square (1 mm × 1 mm) with a quarter sector of a circle (radius $r = 40$ μm) cut out from the corner at the intersection of the symmetry axes. The cylindrical specimen incorporates rotational symmetry and half symmetry, while the plate-like specimen uses quarter symmetry. The free surfaces (top and right surface in reference to Fig. 2) are constrained to uniform normal displacements. This is done by simply coupling the normal displacements of all nodes belonging to each surface. This straightness condition is imposed as a submodeling technique to eliminate any possible model size effects, i.e., the effect of the defect on the free surface displacements. These effects were, however, found to be insignificant with the relatively small defect. The technique was verified by using a larger 3 mm × 3 mm model, which produced effectively identical results. Dimensions of the specimens and a visualization of the symmetry boundary conditions are shown in Fig. 2. To control for the effect of notch plasticity when underloads are considered, models without the cavity/hole are also used. These models incorporate a sharp initial crack of the same size in place of the crack-initiating cavity/hole (see Fig. 3(c)).

3.2. Material model

The modeled specimen comprises of continuous and homogeneous material. However, especially for short cracks, the effect of local microstructure is often very significant (see, e.g., [44]). For this reason, a large scatter is usually present in results considering short cracks. Nevertheless, a homogeneous continuum model can be seen to provide a certain baseline result, around which a varied level of scatter exists. A relevant consequence of the continuum assumption relates to the meaning of short cracks. In a continuous medium, no microstructural short crack effects can exist. Thus, the present work focuses on physically short cracks, referring to the phase of crack propagation where crack closure is developing. Additionally, the proximity to the initial defect is important in terms of the underload response and initial closure development.

Material parameters correspond to a conventional high strength steel. Bilinear material model is used to reduce model complexity. Perfectly kinematic linear hardening is defined for the material model. To control for the effect of hardening behavior, some analyses also incorporate a perfectly isotropic hardening model for comparison. As strains remain relatively low in the present simulation, ultimate tensile strength is not assigned; hardening behavior remains linear for the entire plastic strain range. The hardening ratio is $H/E = 0.05$, where Young's modulus is $E = 210$ GPa and hardening modulus $H = 10.5$ GPa. Poisson's ratio is $\nu = 0.3$. According to a vast array of experimental information analyzed by Murakami et al. [45], fatigue limit is controlled by one material parameter, Vickers hardness HV. For compatibility with the Murakami-Endo fatigue model, the strength property is defined in terms of Vickers hardness, which is chosen to be 300 HV. An empirical relationship between hardness and yield strength, Eq. (1) [46], is used in order to link the Murakami–Endo fatigue limit to the material model used in simulations. Thus, the hardness of 300 HV corresponds to a yield strength of 772.10 MPa.

$$\sigma_y = -90.7 + 2.876HV \tag{1}$$

3.3. Loading and boundary conditions

The boundary conditions for the axisymmetric model include a y-directional symmetry condition on the bottom side (crack plane) and a rotational symmetry condition along the y-axis on the left side, referring to the model orientation and coordinate system in Fig. 3. With the plate-like models, plane stress and plane strain, the left side axisymmetry condition is substituted with a x-directional symmetry condition. The y-directional symmetry condition in the crack plane is incrementally relieved to allow for crack propagation, which is described in more detail in Section 3.5.

A Mode I cyclic load is applied to the top edge of the modeled specimen. As plasticity-induced crack closure has the greatest significance near fatigue limit, loading is chosen to correspond to the fatigue limit

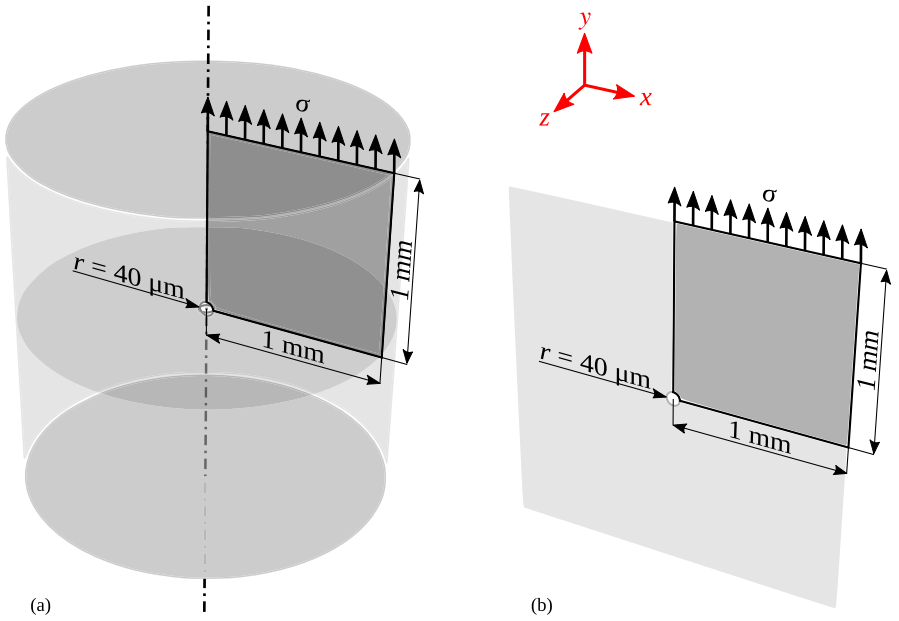

Fig. 2. Schematic visualization of the geometries used; (a) rotationally symmetric specimen model with an internal spherical cavity and (b) plate-like specimen model with a circular hole.

of the Murakami–Endo model [47]. This empirical–analytical fatigue model is shown to predict defect-initiated fatigue limits remarkably well for both internal and surface defects [33,47]. For smooth steel specimens in high and very high cycle fatigue, initiation from small defects, such as non-metallic inclusions, is observed to be the primary fatigue crack initiation mechanism [33,48,49]. The applied stress amplitude is the fatigue limit when controlled by crack propagation from an internal defect, given by Eq. (2). The stress ratio considered in present work is $R = 0$. For the cylindrical specimen, this results in a stress amplitude of 269.69 MPa, maximum and minimum loads being 539.39 MPa and 0 MPa, respectively. For the plate-like specimen, the base loading is simply scaled by a factor of $2/\pi$ to produce a similar stress intensity, resulting in a stress amplitude, maximum stress and minimum stress of 171.69 MPa, 343.38 MPa and 0 MPa, respectively.

$$\sigma_w = \frac{1.56(HV+120)}{(\sqrt{area})^{1/6}}\left(\frac{1-R}{2}\right)^{\alpha}, \quad \alpha = 0.226 + HV \times 10^{-4} \tag{2}$$

The underload effect is investigated by applying a single underload at different stages of crack propagation, namely at normalized crack extensions $a/r = [0.25, 0.5, 0.75, 1.0]$. In most analyses the compressive load spike is applied at the halfway of crack propagation, i.e., at $a/r = 0.75$. The underload magnitude is normalized by the threshold load level for global yielding in compression, σ_{GY}, which deviates from the material yield stress ($\sigma_y = 772.1$ MPa) according to the out-of-plane constraint, as well as the load-carrying cross section area reduction caused by the initial defect. This is done to exactly categorize the analysis conditions into absence or presence of global plasticity, as it was found to have a significant effect on the underload response. Global yielding is defined as the event where the entire cross section in the defect plane is in plasticity. As yielding is defined via the von Mises stress criterion, a higher uniaxial load is required to achieve yielding due to the out-of-plane stress component in plane strain conditions. Secondly, a hole or a cavity reduces the cross-sectional area carrying compression, lowering the uniaxial load required for yielding of the whole cross section. Thus, the global yielding threshold may be expressed as a function of the material yield stress σ_y in the following form:

$$\sigma_{GY} = -\frac{A_{eff}}{A_{nom}}\alpha\sigma_y, \text{ where } \frac{A_{eff}}{A_{nom}} = \begin{cases} 1, & \text{sharp crack} \\ 0.96, & \text{circular hole} \\ 0.9984, & \text{spherical cavity} \end{cases}, \text{ and}$$

$$\alpha = \begin{cases} 1, & \text{plane stress, axisymmetric} \\ 1/\sqrt{\nu^2 - \nu + 1} \approx 1.125, & \text{plane strain} \end{cases}. \tag{3}$$

In Eq. (3), A_{eff} is the effective cross-sectional area carrying compression in the defect plane, A_{nom} is the nominal cross-sectional area to which the external stress is applied at the top surface, and α is the ratio between the uniaxial applied stress and the von Mises equivalent stress. The resulting values of σ_{GY} are provided in Table 2. Underload magnitude is varied in $\sigma_{UL}/\sigma_{GY} = [0.5, 0.6, 0.7, 0.8, 0.9, 1.0, 1.1, 1.2]$. Results are compared to the corresponding constant amplitude results.

3.4. Finite element mesh

The 2D geometry is discretized to a fine, structured mesh of linear quadrilateral elements (CAX4, CPS4 or CPE4, depending on the constraint conditions) near the crack path. The rest of the geometry is meshed freely with the same element type. The four-node elements utilize full integration with four integration points within the element area. The finite element mesh used in the simulations is presented in Fig. 3. The structured mesh section is sized to encase the plastic zone of the growing crack in its entirety at all times except the underload steps, where a single breach into the unstructured mesh was necessary as in some cases the magnitudes of the aforementioned load spikes even exceed the yield strength, inducing global plasticity.

In literature, it is often recommended to base the element size on the theoretical reversed plastic zone size [50,51], or forward plastic zone size [38,52,53]. For accurate evaluation of plasticity-induced crack closure, it is critical that the finite-element mesh is fine enough to appropriately describe reversed plasticity [53]. A common recommendation is that the element size equals at most one tenth of the theoretical forward plastic zone size r_p, which according to the Irwin estimation is given by Eq. (4) [52,54],

$$r_p = \frac{K_{max}^2}{\alpha\pi\sigma_y^2}, \tag{4}$$

where $\alpha = 1$ corresponds to plane stress condition and $\alpha = 3$ to plane strain condition. In a short crack propagation analysis this recommendation is difficult to fulfill as the plastic zone size increases with increasing crack length. If crack propagation begins at zero length without an initial crack, as is the case with the present analysis considering

Table 2
Threshold load levels for global yielding, σ_{GY}, in all of the investigated cases. σ_{GY} is used to normalize the underload magnitudes to separate analyses based on the presence or absence of global plasticity.

Defect	Round			Sharp	
Constraint	Axisymmetric	Plane stress	Plane strain	Axisymmetric or plane stress	Plane strain
σ_{GY} [MPa]	−770.86	−741.22	−833.93	−772.10	−868.68

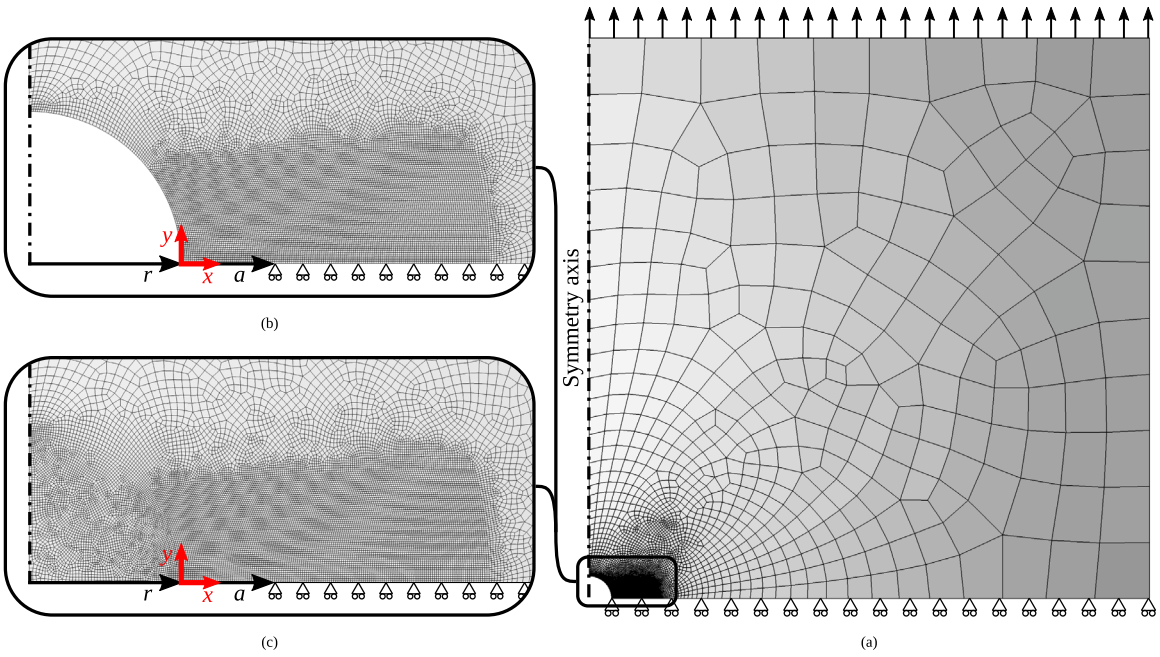

Fig. 3. Visualization of meshing details; (a) 2D geometry and finite element mesh, (b) close-up of the round initial defect and structured mesh section near the crack, and (c) close-up of the mesh with a sharp initial crack in place of the round initial defect.

the round defect, the theoretical plastic zone is initially very small. This results in an overly strict element size requirement, especially when considering the omission of notch plasticity in Eq. (4). In the base model, element size is chosen to be $l_e = 0.5$ μm, which corresponds to $l_e/r_p = 0.1$ near the halfway point of crack propagation if the smaller, plane strain plastic zone estimation is used. This provides continuous and reasonable results, with no abrupt changes observed when decreasing element size further. It is, however, worth pointing out that when analyzing closure level by node contact criterion, the result is intrinsically dependent on element size [41].

3.5. Crack growth scheme

In present analyses, the crack propagates from the defect root to a final length equal to 1.5 times the initial defect's radius. Crack extension a does not include the initial defect. It follows that the chosen total crack extension at the final length crack, $a/r = 1.5$, spans 120 elements or 121 nodes with the chosen element sizes. Crack initiation is assumed as the modeled specimen is loaded at Murakami-Endo fatigue limit, which is empirically characterized by initiating but non-propagating cracks. Stage II propagation is assumed as the crack propagates from a defect, allowing the use of a straight horizontal crack path. Crack propagation-related results, such as level of plasticity-induced crack closure, are not defined before the first propagation increment from a smooth initial defect, which is why the first results are obtained only after the first crack propagation increment at $a = l_e$. Crack propagation is realized by releasing the crack tip node every fourth load cycle. The number of load cycles between the node releases determines the crack growth rate for a given element size. In finite element simulations, crack growth rate is orders of magnitude higher than with real cracks [41]. It is currently infeasible to target realistic crack growth rates in simulations due to the computational cost. Usually at least two load cycles are recommended as propagation at every load cycle can yield artificially elevated closure levels due to the transient plastic strain field [41,55]. Four load cycles are applied here between node releases to find a balance between sufficient plasticity stabilization and computational cost.

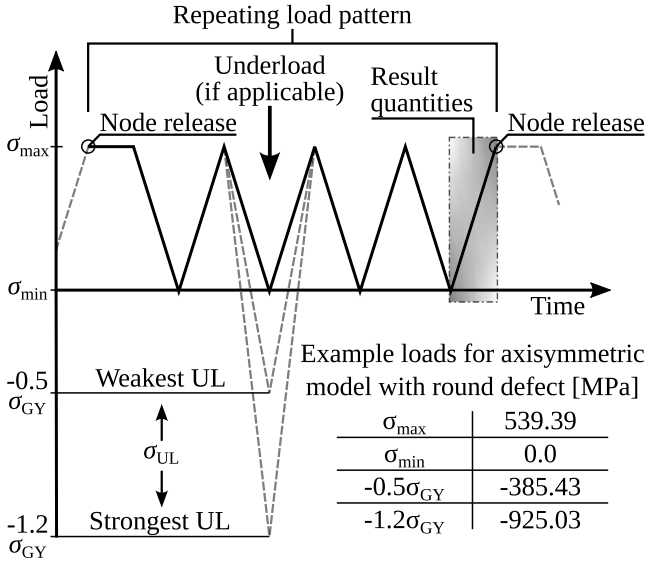

Fig. 4. Schematic representation of the repeating loading sequence proportionally depicting the underload range.

Crack growth takes place at maximum load, which is physically most intuitive in the case of incremental crack propagation, and therefore most commonly used in literature [32,52,55–62]. Another commonly used practice is releasing the crack tip node at minimum load [37,51,63,64], which is physically unrealistic but numerically more stable [37,41]. However, neither method is capable of describing the continuous process of true crack propagation adequately [57]. In literature, the effect of load cycle point at which the crack is allowed to propagate is considered negligible [37,51,53]. However, in the present study, slightly lower closure levels were consistently obtained when crack was allowed to propagate at minimum load, versus maximum load. One of the limitations in the current framework of finite element crack propagation simulations is the discontinuous nature of crack propagation, where propagation increment Δa is defined by element size l_e (i.e., $\Delta a = l_e$) [41]. It is worth noting that releasing at maximum load requires an additional step of maximum load after node release to reach an equilibrium state in the new boundary conditions before load reversal [38]. Depiction of the crack propagation scheme and the repeating loading sequence, comprising of a total of 9 steps, is presented in Fig. 4.

3.6. Contact properties

In crack closure studies it is common practice to use the first node contact criterion, i.e., derive the opening or closing levels based on the contact of first node behind the crack tip. This means that the contact constraint has to accurately represent true contact in the very local node-to-node basis. An analytically rigid, frictionless surface is placed on the crack plane to represent the other half of the crack. Hard contact relationship, which implies no pre-contact stiffness, is used between the crack surface and the rigid surface. Node-to-surface discretization method is used to minimize penetration into the rigid master surface. As penetration takes place, ABAQUS performs severe discontinuity iterations until the penetration is within tolerance. The default contact algorithm in ABAQUS using the direct enforcement method with Lagrange-multipliers demonstrates good performance in achieving a stable and continuous result, provided that the load incrementation is adequately fine. If less than 10 substeps were used per one analysis step, the contact formulation caused instabilities due to too large penetration.

3.7. Output data and performance

Analysis results are obtained via the plastic strain field, crack surface nodal displacements and crack plane element stresses. Post-processing is automated with an ABAQUS–Python script. Most data are gathered from the last loading step before the next node release as illustrated in Fig. 4. This final step in each loading sequence, as well as the unloading step preceding it, is divided into 40 increments each to obtain smoother results. All steps in that loading sequence where the underload is applied also use this finer increment. For all other steps, a dynamic increment of 10 to 100 is defined.

By enquiring the displacement of each node behind the crack tip, a crack profile can be plotted, providing information of not only the crack tip opening displacement (CTOD) values but the opening displacement of the entire crack flank. This can be done at any point during crack propagation to also obtain the crack profile development. Crack surface nodal displacements can also be used to obtain the crack opening or closure level, which serves as a natural indicator of premature crack closure intensity. Multiple different criteria for crack closure are suggested in literature, most common of which are first node contact and tip tension criteria [38,52]. In 2D analyses, first node contact criterion monitors the displacements of the first crack surface node behind the crack tip; if the nodal displacement is zero or below some small threshold value, the crack is considered closed. Tip tension criterion monitors the sign of the axial stress in the current crack tip; if the corresponding axial stress is zero or below, the crack is considered closed. In present work, first node contact criterion was used to acquire the opening level of each node directly behind the propagating crack front. Linear regression in the time–displacement domain was used to obtain the point in time in which nodal displacement was zero. Data points in the analyzed loading step which form a linear part in the time–displacement curve (points with positive, non-zero displacements belonging to approximately the lower third of the total displacement range) were considered in the regression.

To obtain information on the crack residual stress state, the axial stresses ahead or at the crack tip can be investigated at zero external load. Residual stresses are obtained from the crack plane elements up to 10 μm ahead of the crack tip by enquiring the averaged element centroid y-directional stresses at zero load. Plasticity-induced crack closure is by definition a direct result of the specimen plastic strain state. Plastic strains are enquired and visualized in the whole model. Running one analysis on CSC's Puhti supercomputer took approximately 4 h. The number of elements was 21 541. Computation was performed within a single node with 10 cores. Running the single-threaded post-processing script took approximately 5 min.

3.8. Model limitations

Present finite element model carries many assumptions to reduce model variables and decrease computational cost. Present model suffers from many of the same limitations as crack propagation models described in literature [41], which include:

- Model is composed of continuum material, i.e., microstructural heterogeneity is not taken into account.
- Crack propagation is of incremental nature.
- Only closure mechanism taken into account is plasticity-induced crack closure.
- Round defect is modeled as a perfect spherical cavity or circular hole.
- Crack propagation rate is constant and orders of magnitude higher than in reality.
- Crack tip is infinitely sharp.

4. Results

Results from the finite element simulations, as well as some analytical considerations for finite and infinite life fatigue design, are presented in this section.

4.1. Constant amplitude loading

We begin by validating the model in constant amplitude loading considering a sharp initial crack (see Fig. 3(c)). Comparisons to numerical and experimental results found in literature are presented in Fig. 5. It is noteworthy that in the solutions of Refs. [52,55] the abscissa, crack extension, is originally normalized by an analytical plastic zone size, and thus these solutions have been appropriately transformed in order to be plotted in Fig. 5(a). It can be observed that a fair agreement exists between literature reportings and present results regarding the initial development and saturation values of plasticity-induced crack closure. It is noteworthy that a non-monotonic development of σ_{op}/σ_{max} is predicted in axisymmetric and plane strain conditions, whereas the plane stress curve saturates monotonically. The evolution of plasticity-induced crack closure can be captured with a double exponential decay function augmented by a linear and a constant term, Eq. (5). Table 3 presents the curve fitting parameters determined for the opening levels in constant amplitude loading. Quality of fit is assessed with the coefficient of determination, R^2.

$$\frac{\sigma_{op}}{\sigma_{max}}(a/r) = Q_1 e^{-b_1 \cdot a/r} + Q_2 e^{-b_2 \cdot a/r} + c_1 \cdot a/r + c_2 \quad (5)$$

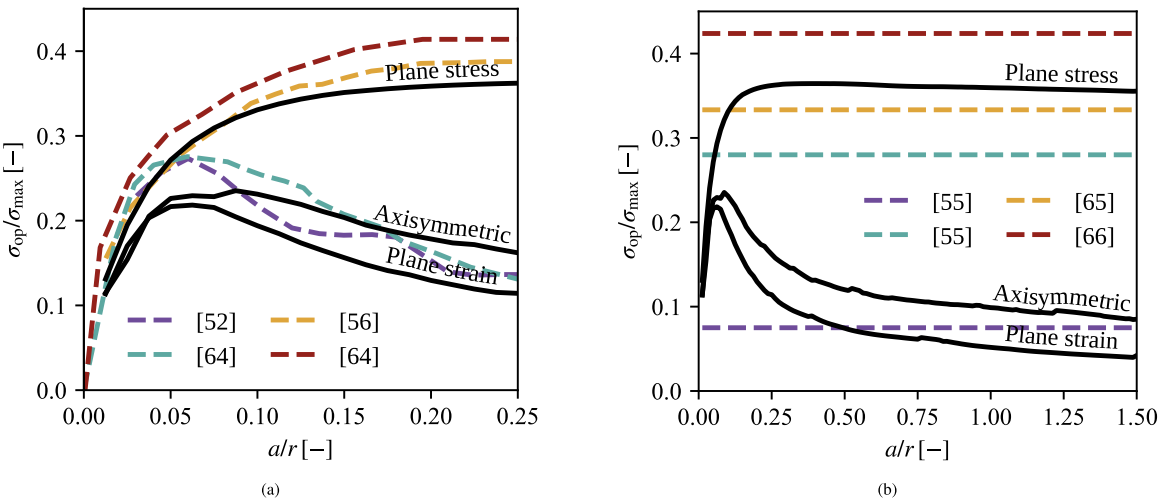

Fig. 5. Literature comparison of opening levels (σ_{op}/σ_{max}) as a function of normalized crack extension (a/r) in constant amplitude loading. (a) Initial development of the opening level versus numerical solutions in plane stress [56,64] and plane strain [52,64] conditions. (b) Opening level saturation versus numerical and experimental stabilized values in plane stress [55,65], [66] as cited in [67], and plane strain [55] conditions. Both subfigures consider the same analyses with a different horizontal scale.

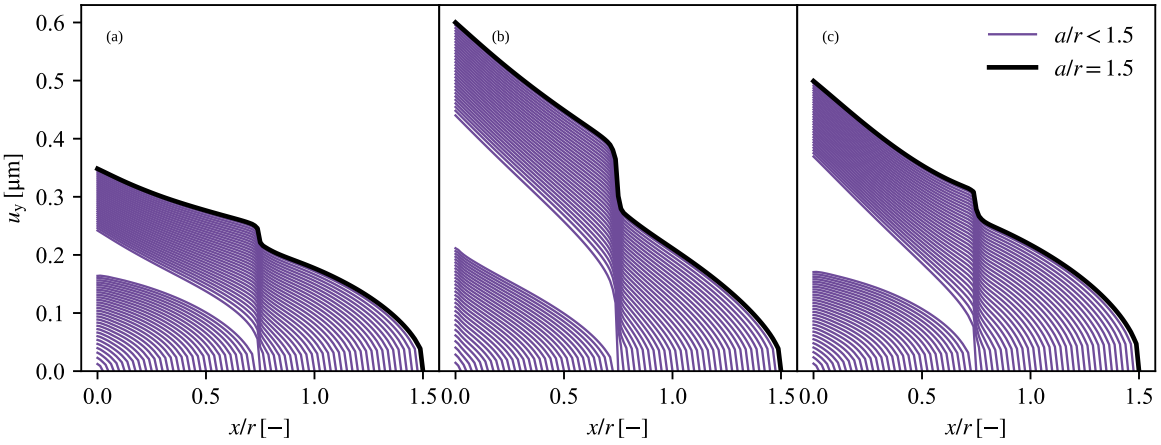

Fig. 6. Crack profile development in (a) axisymmetric, (b) plane stress, and (c) plane strain conditions. A single underload is applied at halfway point of crack propagation, at a normalized crack extension $a/r = 0.75$. Round initial defects are considered. Normalized underload magnitude is $\sigma_{UL}/\sigma_{GY} = 1.0$ (see Table 2). Crack profile is drawn at maximum load at every other crack tip position for better distinction.

Table 3
Parameters for fitting the constant amplitude results to Eq. (5).

Defect	Constraint	Q_1	Q_2	b_1	b_2	c_1	c_2	R^2
Round	Axisymmetric	1.878	−2.067	10.184	13.204	−0.016	0.097	0.995
	Plane stress	−0.055	−0.430	2.143	22.642	−0.001	0.358	0.977
	Plane strain	1.012	−1.206	8.191	13.671	−0.016	0.056	0.988
Sharp	Axisymmetric	0.298	−0.385	7.830	24.898	−0.028	0.127	0.997
	Plane stress	−0.256	−0.068	29.558	11.022	−0.009	0.369	0.999
	Plane strain	0.571	−0.609	11.676	22.632	−0.034	0.088	0.995

4.2. Underload

Results considering single underloads are presented in this section, most of which consider a round initial defect (see Fig. 3(b)). The most intuitive result is perhaps the crack profile, which is examined first by plotting the y-directional nodal displacement, u_y, of crack surface nodes at maximum load. In the crack propagation simulation, the crack profile can be drawn at any crack length. Crack profile development is presented in Fig. 6 for each of the constraint conditions, axisymmetric, plane stress, and plane strain. The effect of the underload applied at the halfway point of crack propagation can be clearly distinguished. The underload, whose magnitude is equal to the global yielding threshold, causes reversed plasticity in the entire crack flank behind the underload crack tip location. In essence, this gives rise to apparent crack tip blunting as clearly seen in Fig. 6, similarly than with an overload [35]. This effect is at its weakest in the axisymmetric case due to a smaller stress concentration factor of the 3D spherical defect compared to the 2D hole, but is also affected by the constraint condition.

4.2.1. Effect of underload magnitude

Underload magnitude is known to have a substantial effect on the subsequent crack propagation behavior. Here, the effect of different underload magnitudes on the following plasticity-induced crack closure levels is investigated by applying underloads of varying magnitude, normalized by the global yielding threshold, at the halfway point of crack propagation (see Table 1). The results for each constraint state are presented in Fig. 7.

Firstly, it can be seen in Fig. 7(a) that instead of lowering the following σ_{op}/σ_{max}, which would be expected considering the literature consensus, the underload clearly strengthens the near-tip plasticity-induced crack closure in axisymmetric conditions. Furthermore, the post-underload opening levels increase approximately monotonically with the underload magnitude. For the plate-like specimens, Fig. 7(b,c), the behavior seems different as σ_{op}/σ_{max} is decreased when weaker underloads are applied. However, the global yielding threshold, σ_{GY},

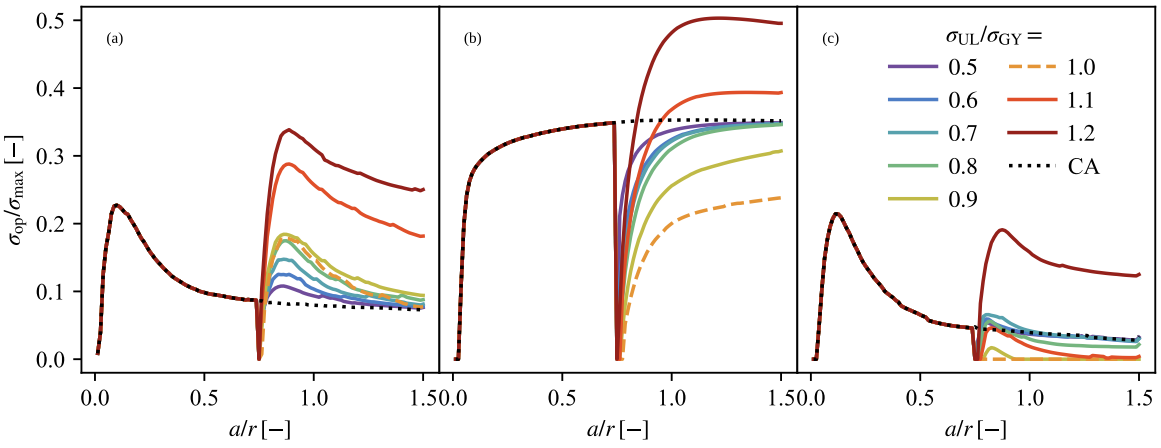

Fig. 7. Opening level (σ_{op}/σ_{max}) as a function of normalized crack extension (a/r) in (a) axisymmetric, (b) plane stress, and (c) plane strain conditions. A single underload is applied at halfway point of crack propagation, at a normalized crack extension $a/r = 0.75$. Round initial defects are considered. Normalized underload magnitude σ_{UL}/σ_{GY} is varied (see Table 2). Constant amplitude (CA) reference is also presented.

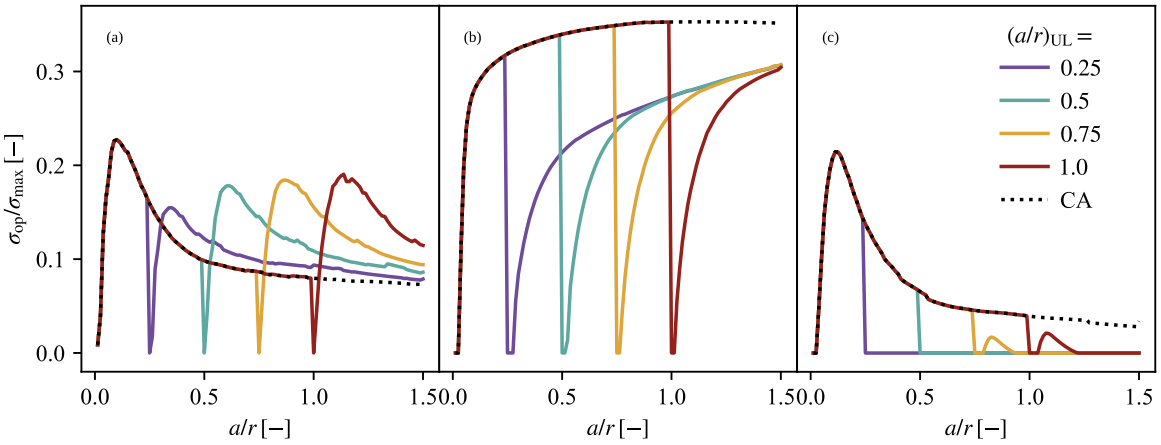

Fig. 8. Opening level (σ_{op}/σ_{max}) as a function of normalized crack extension (a/r) in (a) axisymmetric, (b) plane stress, and (c) plane strain conditions. A single underload is applied at various points of crack propagation denoted $(a/r)_{UL}$. Round initial defects are considered. Normalized underload magnitude is $\sigma_{UL}/\sigma_{GY} = 0.9$ (see Table 2). Constant amplitude (CA) reference is also presented.

seems to mark an important point regarding the underload magnitude. A further increase past this point, highlighted with the dashed line, begins to raise the following σ_{op}/σ_{max}. A sizeable jump can also be observed with the axisymmetric model, Fig. 7(a), once the underload magnitude surpasses σ_{GY}.

It is evident that the propagation distance after underloads is in some cases shorter than what would be required to re-stabilize the opening levels. However, according to preliminary simulations considering larger propagation distances, all results with underload magnitudes below the global yielding threshold tend asymptotically towards the constant amplitude result after the analysis window chosen herein. Results with underload magnitudes surpassing the global yielding threshold find a new, higher saturation value due to the mechanism discussed later in Section 5.1.3. The initial transient after the underload, which bears the most significance in terms of the present study, is nevertheless captured.

4.2.2. Effect of underload location

In order to assess the effect of crack length at the time of the underload, underloads are also applied at different stages of crack propagation, i.e., at differing crack tip locations. This is done to evaluate underload effects in physically short cracks, determining the possible trend in underload behavior with decreasing crack length. The results for each constraint state are presented in Fig. 8. It can be observed that the earlier the underload is applied, the lower the following opening levels become. This effect seems to diminish further away from the initial defect, meaning that for a sufficiently long crack the crack length at the time of the underload no longer affects the underload response.

4.2.3. Effect of initial defect type

The combination of the constant amplitude external load and the stress concentration of the initial defects result in tensile notch plasticity in the defect root. The local and nominal y-directional stress ranges in the crack path prior to crack propagation are shown in Fig. 9 for all three constraint conditions. From the discontinuity in the local stress curves, the extent of notch plasticity can be observed. The local stress ratio is also slightly affected by notch plasticity, reducing down to $R \approx -0.2$ in axisymmetric and plane stress, and approximately $R \approx -0.1$ in plane strain conditions. In addition to having an effect in tensile loading, the same stress concentration of the round defects is active for the compressive underloads. Considering this, compressive notch plasticity induced by the round defects during the underload may be significant.

As the proximity of the crack tip to the initial defect at the time of the underload had an effect on the resulting opening levels, as seen in Fig. 8, it is conceivable that the initial defect geometry is also significant in terms of the underload response in short cracks. To verify this, cracks propagating from a round initial defect (Fig. 3(b)) are compared to those propagating from a sharp initial crack (Fig. 3(c)) in terms of the opening level underload response. Fig. 10 presents the

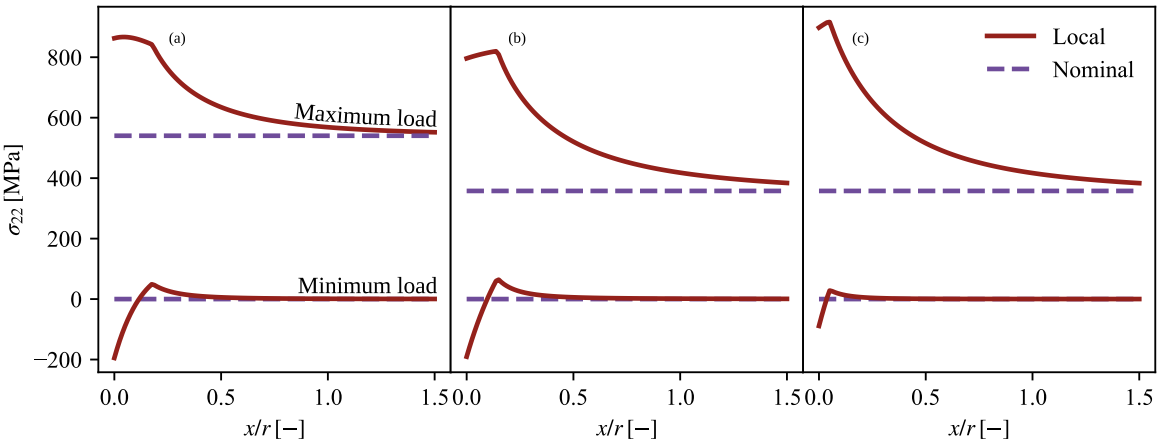

Fig. 9. Local and nominal y-directional stresses (σ_{22}) as a function of the normalized crack path coordinate (x/r) prior to crack extension in (a) axisymmetric, (b) plane stress, and (c) plane strain conditions.

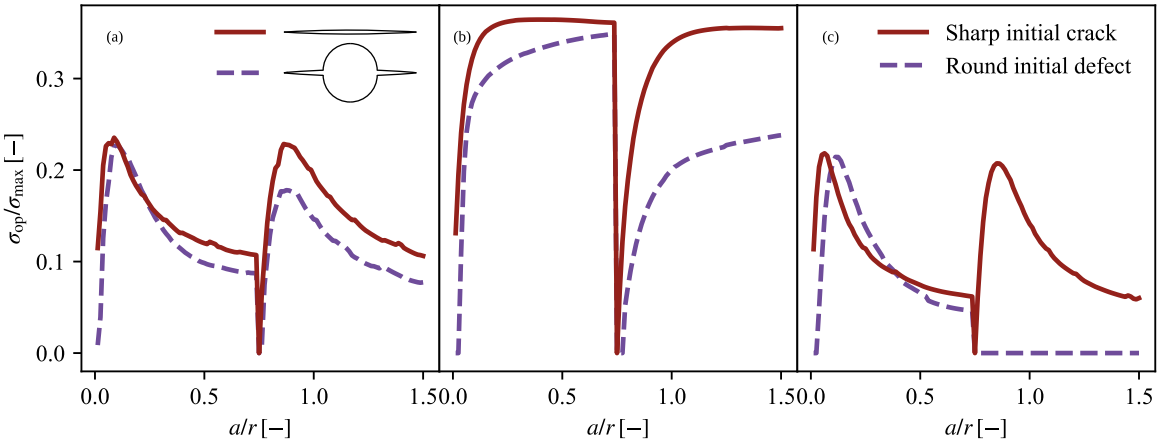

Fig. 10. Opening level (σ_{op}/σ_{max}) as a function of normalized crack extension (a/r) in (a) axisymmetric, (b) plane stress, and (c) plane strain conditions. Normalized underload magnitude is $\sigma_{UL}/\sigma_{GY} = 1.0$ (see Table 2).

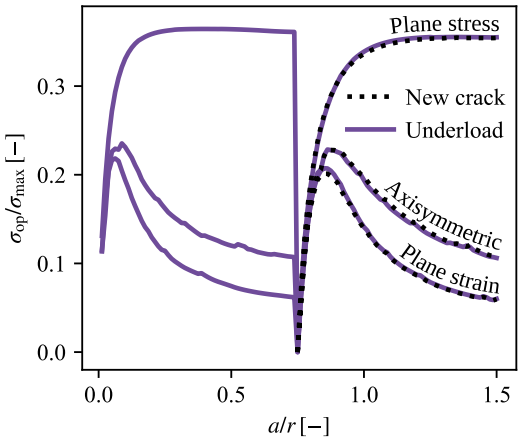

Fig. 11. Opening level development after the underload compared to that of a new, load-history-free crack under constant amplitude loading. Normalized underload magnitude is $\sigma_{UL}/\sigma_{GY} = 1.0$ (see Table 2). Sharp initial cracks are considered.

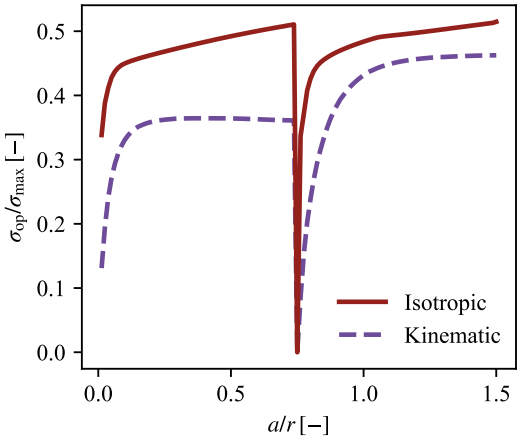

Fig. 12. Opening level development comparing perfectly kinematic and perfectly isotropic hardening in plane stress conditions. Normalized underload magnitude is $\sigma_{UL}/\sigma_{GY} = 1.2$ (see Table 2). Sharp initial cracks are considered.

comparison for each constraint state. The effect of the initial defect type appears substantial. The reduction of σ_{op}/σ_{max} after the underload is no longer observed with the plate like specimens if a sharp initial crack is used in place of the round initial defect. Increased opening levels are also predicted in the axisymmetric specimen with the sharp initial crack, although the 3D defect is much less sensitive to the change. If the compressive notch plasticity caused by the underload is eliminated by using the sharp initial crack, the underload seems to only cause what is essentially a resetting of the opening level development. A

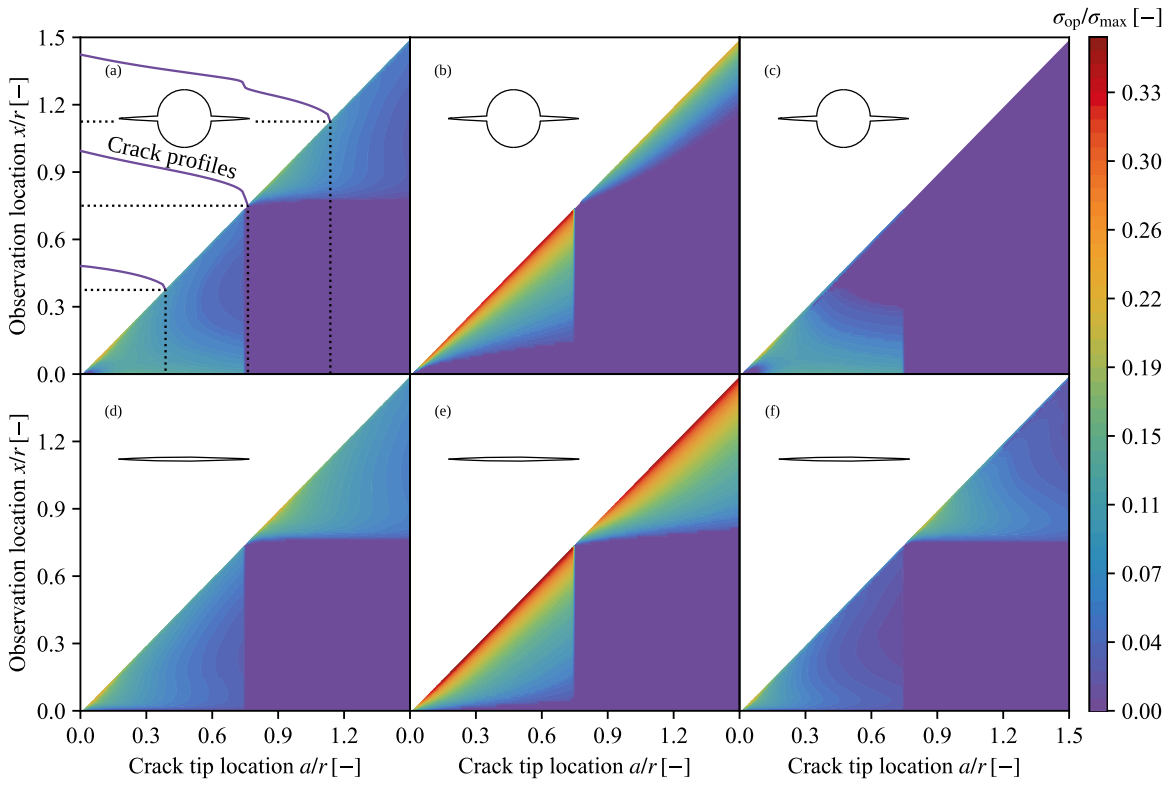

Fig. 13. Opening level (σ_{op}/σ_{max}) as a function of normalized crack extension (a/r) and location on the crack surface (x/r). Initial defect is (a,b,c) round defect and (d,e,f) sharp crack. Constrain condition is (a,d) axisymmetric, (b,e) plane stress, and (c,f) plane strain. A single underload is applied at halfway point of crack propagation, at a normalized crack extension $a/r = 0.75$. Normalized underload magnitude is $\sigma_{UL}/\sigma_{GY} = 1.0$ (see Table 2). Three maximum load crack opening profiles corresponding to vertical lines in the contour are drawn in (a) for reference (see Fig. 6).

slight difference is also observed in the first half of propagation under constant amplitude loading between the initial defect types.

Considering the sharp initial crack, the opening level development after the underload can be compared to that of a new crack without any loading history, propagating under constant amplitude loading. Growth of the new crack is started at the same point where the underload is applied in the underload analysis, i.e., the initial crack is an additional $a/r = 0.75$ longer. This comparison is presented in Fig. 11. It can be seen that the opening level development after an underload is nearly identical to that of a new crack devoid of any loading history. This applies to all constraint conditions, given a sharp initial crack, an underload magnitude equal to the global yielding threshold, and kinematic hardening. The underload is capable of essentially removing the effect of loading history (see Section 5.1.1).

4.2.4. Effect of hardening behavior

Fig. 12 shows a comparison of the opening level responses to a high-magnitude underload ($\sigma_{UL}/\sigma_{GY} = 1.2$) using both perfectly kinematic and perfectly isotropic hardening models in plane stress conditions, considering sharp initial cracks. It is evident that the sharp increase in post-underload opening levels when σ_{GY} is surpassed, observed also in Fig. 7, is not present with isotropic hardening. Notice also the difference of constant amplitude opening levels between the hardening models; it is clear that, at least for steels in cyclic loading, perfectly isotropic hardening may overestimate plasticity-induced crack closure due to a lack of reversed plasticity in the crack tip.

4.2.5. Far-field closure

To evaluate plasticity-induced crack closure, usually only the displacement of the first node behind the crack tip is monitored, as it should have the largest influence on the crack tip damage accumulation. It is clear that far-field contact also affects crack propagation to a degree, and total closure influence should be an integral quantity, a weighted sum of the contact over the entire crack surface, but crack closure models incorporating far-field contact considerations have yet to see wider use (see, e.g., [26,68]). In Fig. 13, levels of plasticity-induced closure for the entire crack surface are presented, comparing the underload response with the different initial defect types and constraint conditions. The opening level for every node behind each crack tip position forms a contour figure in the shape of a triangle, as $x/r < a/r$, i.e., closure cannot be observed in front of the crack tip. Line $x/r \approx a/r$ (technically $(x + l_e)/r = a/r$) corresponds to the opening level of the first node behind the crack tip, presented more conventionally in Fig. 10. Line $x/r = 0$ corresponds to the opening level at the initial defect edge. A vertical line from a point on the diagonal line $x/r \approx a/r$ down to $x/r = 0$ thus corresponds to a path from the crack tip to the defect edge on the crack surface. To bring context to the figure, Fig. 13(a) includes three crack opening profiles, also presented in Fig. 6(a), corresponding to vertical lines in the contour. In all cases presented in Fig. 13, all built-up closure disappears from behind the crack tip position where the underload was applied, effectively forming a closure-free crack [69]. This can be attributed to the apparent crack tip blunting, which takes place not only with overloads but with underloads also (see Fig. 6).

4.2.6. Residual stress

Besides crack closure, underload effects have also been commonly explained through the changes in residual stresses ahead of the crack tip, as discussed in the introduction. To examine the residual stress state at and in front of the crack tip, the y-directional stress is determined at zero external load in crack plane elements $[0, 10]$ μm in front of the crack tip for each crack tip position within the propagation. Fig. 14 compares the normalized y-directional residual stress for different initial defect types and constraint conditions.

It can be seen that the residual stress state recovers very quickly after the underload with the instant re-emergence of the crack tip

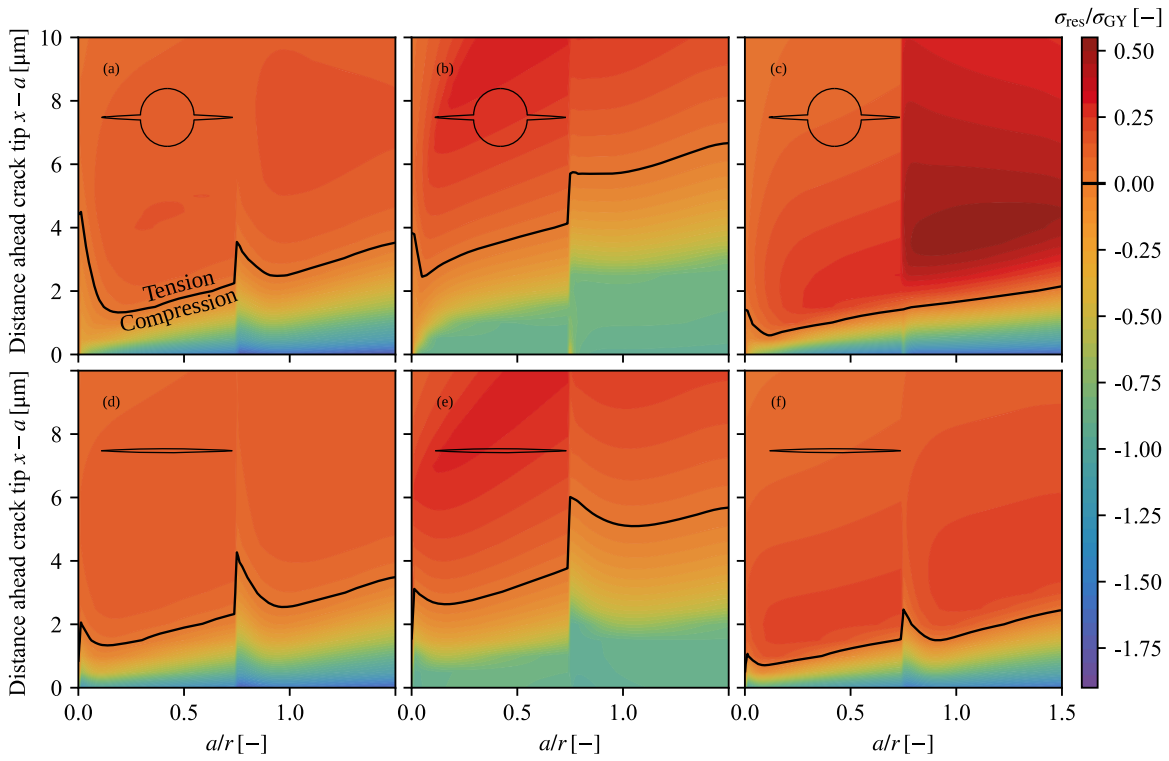

Fig. 14. Normalized residual stress in y-direction (σ_{res}/σ_{GY}) as a function of normalized crack extension (a/r) and location ahead of the crack tip ($x - a$) at zero external load. Initial defect is (a,b,c) round defect and (d,e,f) sharp crack. Constrain condition is (a,d) axisymmetric, (b,e) plane stress, and (c,f) plane strain. A single underload is applied at a normalized crack extension $a/r = 0.75$. Normalized underload magnitude is $\sigma_{UL}/\sigma_{GY} = 1.0$ (see Table 2).

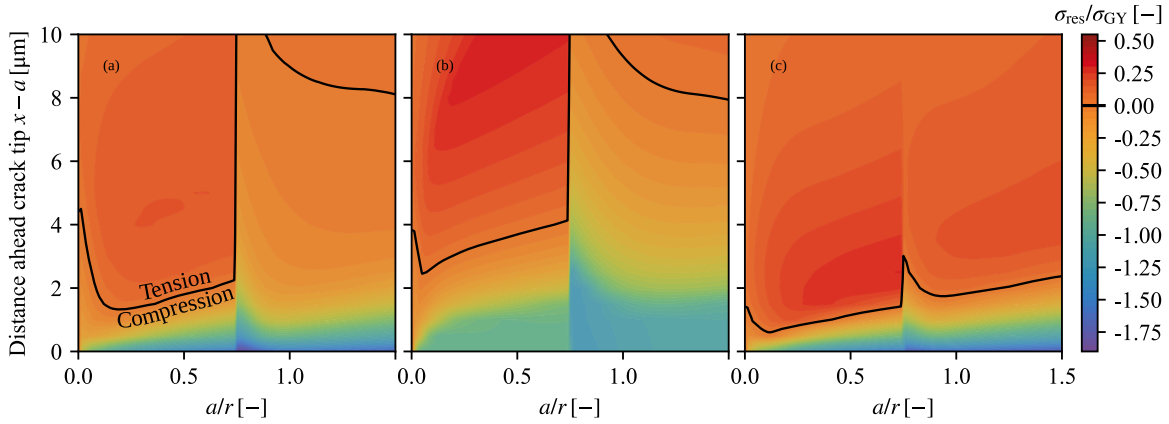

Fig. 15. Normalized residual stress in y-direction (σ_{res}/σ_{GY}) as a function of normalized crack extension (a/r) and location ahead of the crack tip ($x - a$) at zero external load. Round initial defects are considered. Constrain condition is (a) axisymmetric, (b) plane stress, and (c) plane strain. A single underload is applied at a normalized crack extension $a/r = 0.75$. Normalized underload magnitude is $\sigma_{UL}/\sigma_{GY} = 1.2$ (see Table 2).

plastic zone in continued loading. No significant tensile residual stresses are observed after the underload, except with the holed plane strain specimen, Fig. 14(c). The harmful, acceleration-facilitating residual stress transients near the crack tip, if any, are very short-lived, as was also concluded in [24]. Considering axisymmetric specimens and all specimens with the sharp initial cracks, Fig. 14(a,d,e,f), the underload actually slightly strengthens the compressive residual stresses in subsequent loading. The immediate peak of the compressive residual stress, best seen in the axisymmetric conditions, Fig. 14(a,d), can be attributed to the already discussed apparent crack tip blunting, where less of the crack flank is carrying the closing force after the underload.

Further, Fig. 15 considers the residual stress response in the case of underloads of higher magnitude, $\sigma_{UL}/\sigma_{GY} = 1.2$, and round initial defects. It can be observed that even with large underloads, no significant tensile residual stresses are formed in front of the crack tip. In fact, the opposite is true; the residual stress state seems to shift more towards compression.

For a more quantitative representation of the change in residual stress states, Fig. 16 presents the normalized residual stress ahead of the crack tip before and after the underload. The curves before the underload correspond to a crack tip location 1 μm behind, and the curves after 1 μm ahead of the underload crack tip location of $a/r = 0.75$. The general tendency of an underload to strengthen the compressive residual stress ahead of the crack tip is evident, suggesting a reduction of crack driving force. An increase of the residual stress towards tension is seen only with the intermediate underload ($\sigma_{UL}/\sigma_{GY} = 1.0$) and the round initial defect in plane strain, as well as in plane stress in the immediate vicinity of the crack tip.

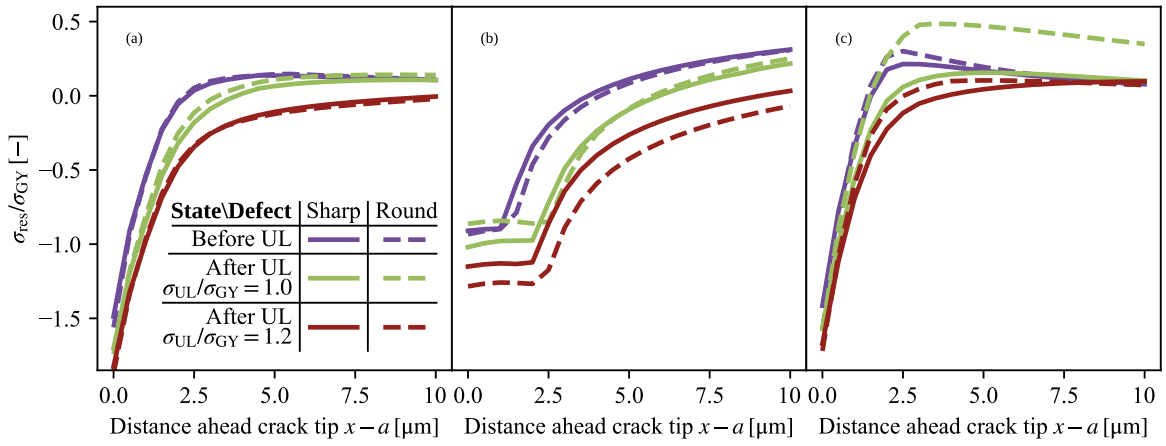

Fig. 16. Normalized residual stress in y-direction (σ_{res}/σ_{GY}) as a function of location ahead of the crack tip ($x-a$) at zero external load before and after an underload. Constrain condition is (a) axisymmetric, (b) plane stress, and (c) plane strain.

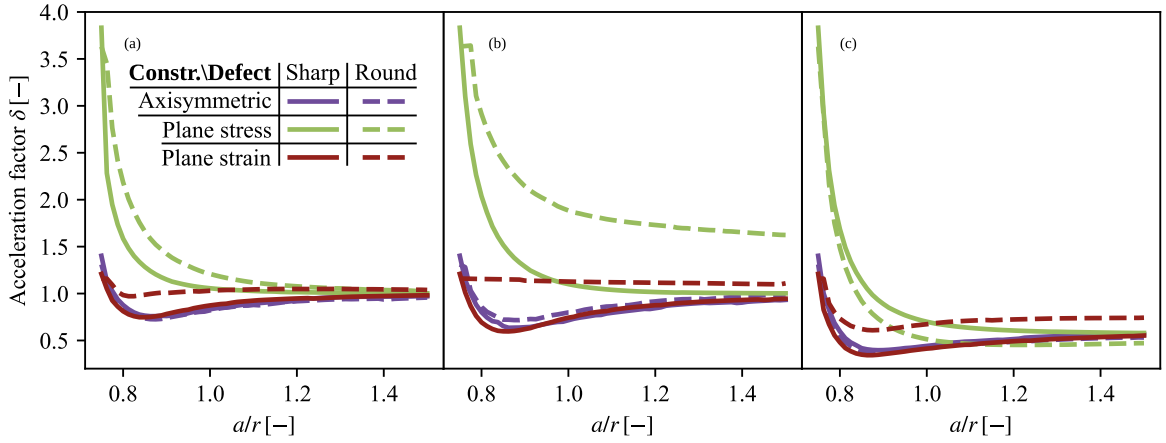

Fig. 17. Acceleration factor (δ) as a function of normalized crack extension (a/r) after an underload is applied at $a/r = 0.75$. Normalized underload magnitude is (a) $\sigma_{UL}/\sigma_{GY} = 0.8$, (b) $\sigma_{UL}/\sigma_{GY} = 1.0$, and (c) $\sigma_{UL}/\sigma_{GY} = 1.2$ (see Table 2).

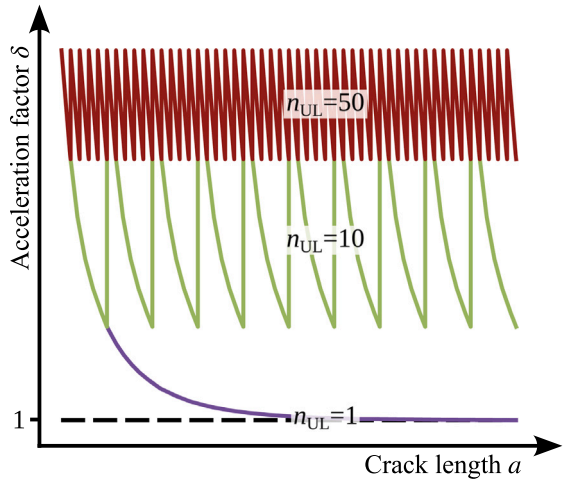

Fig. 18. Schematic illustration of the reconstruction of δ for numerous underloads.

4.3. Effect of underloads on fatigue life

In terms of finite life fatigue design, it can be beneficial to estimate the underload response in terms of the crack growth rate, $\mathrm{d}a/\mathrm{d}N$. A rough estimate can be easily given by the Elber–Paris equation, Eq. (6) [2]. The transient behavior of plasticity-induced closure is taken into account by the effective stress intensity factor range, ΔK_{eff}, which can be expressed according to Eq. (7), [34]. As the Paris parameters C and m, and the maximum stress intensity factor K_{max} are the same between the constant amplitude and underload situations, a ratio of the growth rates, denoted as the acceleration factor, δ, can be derived into the form shown in Eq. (8). It is worth noting that the current analysis conditions are outside the region of applicability of linear elastic fracture mechanics as the short crack may not fulfill the small-scale yielding condition. The use of the Elber correction [1] and ΔK_{eff} allow for extending the applicability of the fracture-mechanical analysis, albeit additional plasticity corrections to ΔK may also be required. The similitude concept is generally thought to apply for the parameter ΔK_{eff} [34]. Nevertheless, the present analysis does not rely on exact values of stress intensity factors. It is only assumed that the K_{max} in Eq. (7) is unchanged by an underload, and thus cancels out in the ratio of Eq. (8).

$$\mathrm{d}a/\mathrm{d}N = C\left(\Delta K_{eff}\right)^m \tag{6}$$

$$\Delta K_{eff} = K_{max}\left(1-\sigma_{op}/\sigma_{max}\right) \tag{7}$$

$$\delta = \frac{(\mathrm{d}a/\mathrm{d}N)_{UL}}{(\mathrm{d}a/\mathrm{d}N)_{CA}} = \left(\frac{1-(\sigma_{op}/\sigma_{max})_{UL}}{1-(\sigma_{op}/\sigma_{max})_{CA}}\right)^m \tag{8}$$

Acceleration is predicted if $\delta > 1$, and deceleration if $\delta < 1$. Post-underload evolution of δ is shown in Fig. 17 for all constraint

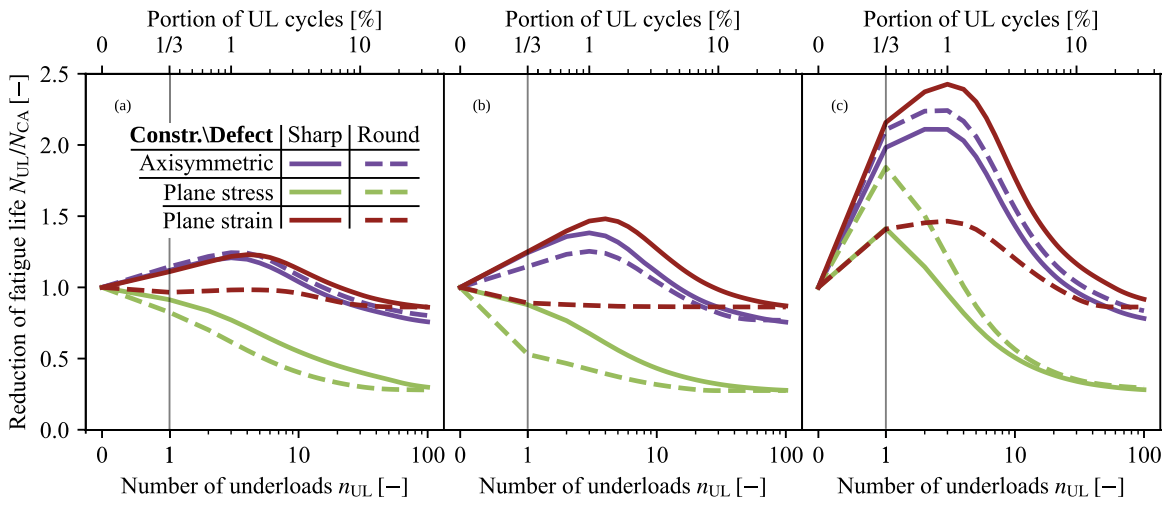

Fig. 19. The reduction of fatigue life (N_{UL}/N_{CA}) as a function of the number of underloads (n_{UL}) within the crack propagation interval $a/r = [0.75, 1.5]$. The range between zero and one in n_{UL} is shown on a linear scale. For a given mean growth rate, 1e-7 m/cycle used here as an example, the abscissa can be transformed into a percentage of underload cycles in the loading. Normalized underload magnitude is (a) $\sigma_{UL}/\sigma_{GY} = 0.8$, (b) $\sigma_{UL}/\sigma_{GY} = 1.0$, and (c) $\sigma_{UL}/\sigma_{GY} = 1.2$ (see Table 2).

conditions and defect types, assuming a Paris exponent, $m = 3$, for the sake of simplicity. Three different values of normalized underload magnitude, $\sigma_{UL}/\sigma_{GY} = [0.8, 1.0, 1.2]$, are considered. It is evident that strong initial acceleration is predicted in plane stress conditions, whereas in axisymmetric and plane strain conditions the behavior is mostly deceleration. The response is much stronger in plane stress than in the other constraint conditions, consistent with the plane stress dominated overload behavior observed in [7]. With a lower underload magnitude, a faster recovery to the baseline growth rate is predicted, in accordance with experimental data [21]. Persistent deceleration across all constraint conditions and defect types is predicted with the highest-magnitude underload. If the constant amplitude crack growth rate is known, growth rate after an underload can be estimated by a simple multiplication with δ. In plane stress dominated cases, the result of Fig. 17 can be considered reasonably descriptive of the actual behavior as strong plasticity-induced closure in plane stress can be thought to control the overall closure influence. However, other closure mechanisms can become meaningful especially in plane strain, as the lower level of plasticity-induced closure and usually larger surface area of the plane strain regions can facilitate higher levels of roughness- and oxide-induced closure before the contact points begin to plastically compress at minimum load. Additionally, oxide accumulation occurs mostly on the plane strain regions of the crack [70]. As the removal of all existing closure is expected with underloads, the axisymmetric and plane strain results in Fig. 17, only accounting for plasticity-induced closure, may be unconservative. The curves considering a sharp initial crack may be more suited to finite, and those of round initial defect to infinite life design, due to differences in the characteristic crack length.

This result can be processed further to assess the effect of underloads on fatigue life. The reduction of withstood load cycles can be obtained by integrating the inverse function of δ over the interval $a/r = [0.75, 1.5]$. The result was verified by a numerical simulation of incremental crack advance according to Eq. (8). Note that the δ-curves in Fig. 17 consider only a single underload. To account for numerous underloads, the following assumptions are made:

- Underloads are evenly spaced over the simulated crack propagation window.
- Subsequent underloads behave similarly as the first underload, and thus the δ-curve corresponding to multiple underloads can be constructed by reusing the single underload curve (Fig. 17), shifted along a.

As numerous underloads do not carry a cumulative effect [26] as already discussed in the introduction, the latter assumption is considered valid. The reconstruction of δ for numerous underloads is presented schematically in Fig. 18. The reduction in the number of withstood load cycles in the interval $a/r = [0.75, 1.5]$, N_{UL}/N_{CA}, as a function of the number of underloads within said interval, n_{UL}, is shown in Fig. 19 for all constraint conditions and defect types, similarly to Fig. 17. Three different values of normalized underload magnitude, $\sigma_{UL}/\sigma_{GY} = [0.8, 1.0, 1.2]$, are considered. By assuming a mean growth rate, the result may be presented in terms of a percentage of underload cycles in the loading. These results clearly indicate that, even if an occasional underload could improve fatigue life, frequently repeated underloads are still detrimental due to the initial loss of closure, in line with [8]. In the cases where a post-underload increase in plasticity-induced closure is predicted, a local maximum in fatigue life can be found for a specific underload frequency. Care must be taken in any attempt to generalize the results, since other closure mechanisms, different base loading magnitudes and stress ratios, for example, may have a substantial influence on fatigue life. Additionally, it must be kept in mind that the result is based on a limited analysis window of a short crack after an underload. Generalization to larger crack lengths and less frequent underloads than one per the present simulation window may fail.

4.4. Effect of underloads on fatigue limit

Based on the findings made in this study and especially the load history and closure removal demonstrated in Figs. 11, 13 and discussed later in Section 5.1.1, the effect of underloads can be analyzed in a simple and effective manner using the cyclic resistance curve, or R-curve [71,72]. This provides a basis for infinite life design in applications where underloads can occur. As the load history of a crack can be effectively reset by an underload, and all existing closure is most likely lost, a resetting of the R-curve can also be assumed. This essentially causes a shift of the R-curve towards a higher crack length, lowering the fatigue limit, which is defined by a tangent condition of the ΔK-curve imposed by the loading and the R-curve ΔK_{th}. Based on this consideration, the effective fatigue limit, reduced by a single or numerous underloads can be computed as a function of the number of underloads, n_{UL}. The following assumptions are made to simplify the analysis:

- The R-curve starts anew at the crack length where an underload is applied.
- An underload is applied at the point marking crack arrest, i.e., the intersection point of the ΔK-curve and R-curve. A sporadic underload is most likely experienced when the crack is arrested.

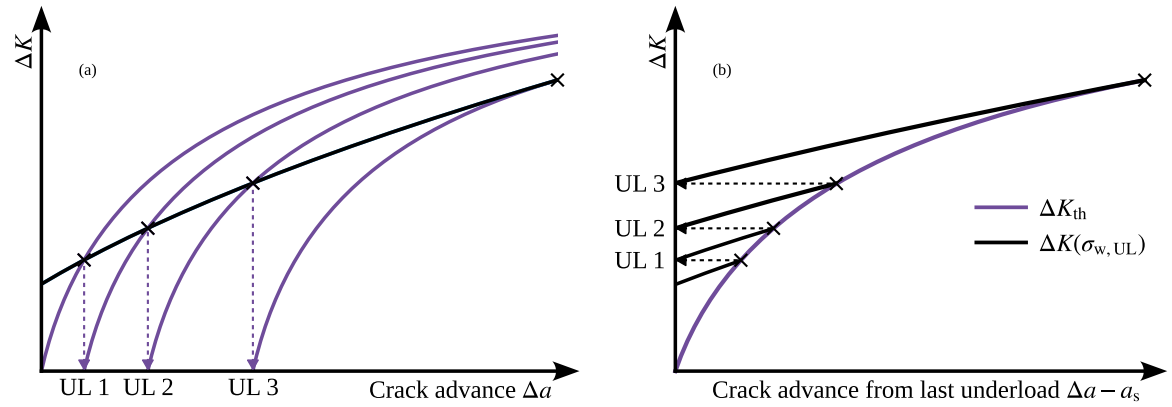

Fig. 20. Schematic illustration of underload analysis by using the cyclic resistance curve. A loading history containing three sporadic underloads is considered in this instance. An underload can be thought to (a) reset the R-curve or (b) transform the crack into a new initial crack.

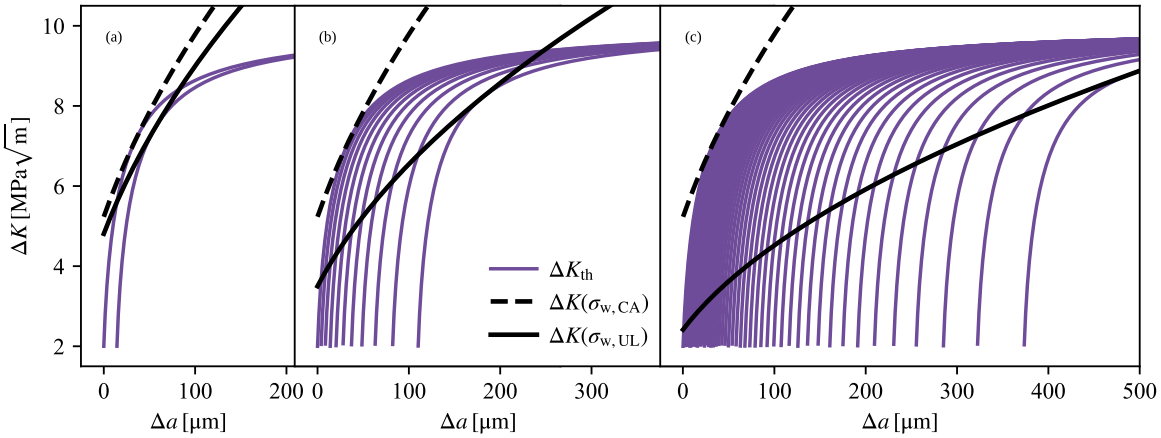

Fig. 21. Cyclic resistance curve development and subsequent decrease of the fatigue limit when the loading history contains (a) 1, (b) 10, and (c) 50 underloads. Resistance curve resets whenever an underload occurs. An underload occurs at each ΔK-curve and R-curve intersection point.

This can be schematically illustrated in one of two ways presented in Fig. 20: by drawing a new R-curve starting at each underload point (Fig. 20(a)), or by shifting the x-axis by the crack extension prior to the underload and taking the post-underload crack as a new, closure-free initial crack (Fig. 20(b)). An underload can be thought to reset the R-curve or transform the crack into a new initial crack, which are functionally the same event. In [71] it is schematically illustrated that a similar resetting of the R-curve is presumed to occur with underloads due to the momentary loss of closure. The described procedure is also supported by the practice of compressive pre-cracking commonly used in experimental works to produce a closure-free initial crack [71].

A condition for crack arrest in terms of R-curve analysis is the equality of ΔK and cyclic R-curve ΔK_{th} [71],

$$\Delta K = \Delta K_{\mathrm{th}} \Leftrightarrow \begin{cases} 2\sigma Y\sqrt{\pi\left(a_{\mathrm{init}}+\Delta a\right)} = \Delta K_{\mathrm{th,lc}}\sqrt{\frac{\Delta a+a^*-a_{\mathrm{s}}}{\Delta a+a^*+a_0-a_{\mathrm{s}}}} \\ a^* = \frac{a_0\left(\Delta K_{\mathrm{th,eff}}/\Delta K_{\mathrm{th,lc}}\right)^2}{1-\left(\Delta K_{\mathrm{th,eff}}/\Delta K_{\mathrm{th,lc}}\right)^2},\ a_0 = \frac{1}{\pi}\left(\frac{\Delta K_{\mathrm{th,lc}}}{Y\Delta\sigma_{\mathrm{th},0}}\right)^2 \end{cases}, \tag{9}$$

where σ is the nominal stress amplitude, Y shape factor, a_{init} initial crack length, Δa crack advance, $\Delta K_{\mathrm{th,lc}}$ long crack threshold stress intensity factor range, $\Delta K_{\mathrm{th,eff}}$ intrinsic threshold stress intensity factor range, and $\Delta\sigma_{\mathrm{th},0}$ material threshold stress range. A new parameter, a_{s}, is introduced, which shifts the R-curve by a length equal to Δa of the previous arrested crack. To evaluate the fatigue limit, ΔK must be a tangent of the final R-curve. As Eq. (9) transforms into a second order polynomial equation, the tangent condition is simply

$$b_2^2 - 4b_1b_3 = 0, \text{ where } \begin{cases} b_1 = 4\pi\sigma_{\mathrm{w}}^2Y^2 \\ b_2 = \left(a_0+a^*+a_{\mathrm{init}}-a_{\mathrm{s}}\right)b_1 - \Delta K_{\mathrm{th,lc}}^2 \\ b_3 = \left(a_0+a^*-a_{\mathrm{s}}\right)a_{\mathrm{init}}b_1 - \left(a^*-a_{\mathrm{s}}\right)\Delta K_{\mathrm{th,lc}}^2 \end{cases}. \tag{10}$$

As the problem of finding $\sigma_{\mathrm{w}}(n_{\mathrm{UL}})$ is recursive in nature, no closed form solution exists. However, the numerical implementation is rather simple. To demonstrate the model, Fig. 21 presents visually the development of the cyclic R-curve ΔK_{th}, and the tangential ΔK defining the fatigue limit when the loading history contains 1, 10, and 50 underloads. The parameter values used are $Y = 1$, $a_{\mathrm{init}} = 40$ μm, $\Delta K_{\mathrm{th,lc}} = 10\ \mathrm{MPa}\sqrt{\mathrm{m}}$, $\Delta K_{\mathrm{th,eff}} = 2\ \mathrm{MPa}\sqrt{\mathrm{m}}$, and $\Delta\sigma_{\mathrm{th},0} = 2 \cdot 1.6\ \mathrm{HV} = 960$ MPa. It is already evident from the increasing difference between the constant amplitude and underload stress intensity factor curves, $\Delta K(\sigma_{\mathrm{w,CA}})$ and $\Delta K(\sigma_{\mathrm{w,UL}})$, that the fatigue limit is reduced more for a larger number of underloads.

Fig. 22 presents the reduction of σ_{w} in terms of the ratio to the constant amplitude fatigue limit, $\sigma_{\mathrm{w,CA}}$, as a function of the number of underloads, n_{UL}. The saturation values obtained from Eq. (11) are also plotted with dashed lines. Three different initial crack sizes, $a_{\mathrm{init}} = [20, 40, 80]$ μm are used to demonstrate a defect size dependency. It can be seen that $\sigma_{\mathrm{w,UL}}/\sigma_{\mathrm{w,CA}}$ saturates with a large enough number of underloads in the loading history. The limit value of σ_{w} is governed by the intrinsic threshold $\Delta K_{\mathrm{th,eff}}$ (see Eq. (11)); once σ_{w} is lowered enough for the initial ΔK to equal $\Delta K_{\mathrm{th,eff}}$, no crack propagation occurs.

$$\lim_{n_{\mathrm{UL}}\to\infty}\sigma_{\mathrm{w}}(n_{\mathrm{UL}}) = \frac{\Delta K_{\mathrm{th,eff}}}{2Y\sqrt{\pi a_{\mathrm{init}}}} \tag{11}$$

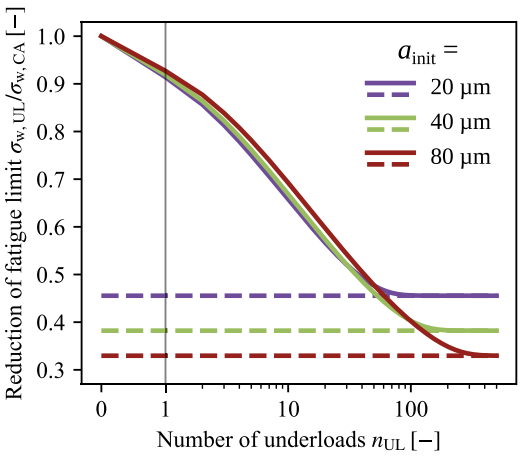

Fig. 22. The reduction of fatigue limit ($\sigma_{w,UL}/\sigma_{w,CA}$) as a function of the number of underloads (n_{UL}) for three different initial crack sizes. Corresponding analytical limit values from Eq. (11) are drawn with dashed horizontal lines for validation. The range between zero and one is shown on a linear scale.

The rate of saturation as a function of n_{UL} depends on the initial value of ΔK at constant amplitude fatigue limit. Thus, faster saturation and decreased sensitivity to repeated underloads is expected from smaller initial defects and lower values of long crack threshold $\Delta K_{th,lc}$. Eq. (11) conservatively estimates the fatigue limit amplitude under numerous underloads, and is easily adapted to many crack/specimen configurations. It should be noted that even a safety factor of 3 to the constant amplitude fatigue limit can be required in underload-heavy applications, as is evident from Fig. 22. It is worth keeping in mind that the analysis presented above assumes a universal R-curve, meaning that the R-curve parameterization provided in [71] is assumed to be valid for short initial cracks also. There is currently limited proof for the applicability of the same R-curve to short initial cracks, although it has been used in this setting before [73]. Nevertheless, it can be presumed that an R-curve of some variety must exist for short initial cracks also. The analysis described in this section primarily presents a novel method of relating underloads to the fatigue limit, and the exact shape of the R-curve is of secondary importance.

5. Discussion

5.1. Mechanisms behind the predicted underload behavior

As is evident from the results, the underload response even in a continuum elastic–plastic crack propagation model is not straightforward. Even the qualitative effect is dependent on constraint conditions, underload magnitude, hardening behavior, and for short cracks, initial defect type. Thus, a detailed examination of the underlying mechanisms is needed to understand the phenomenon. In this section, the authors point out three independent physical mechanisms, a varying combination of which controls the underload response of the continuum short crack model. As mentioned in the last section, the present analysis considers only zero–tension baseline loading. However, all mechanisms discussed here should also apply for other stress ratios. Assuming a constant underload magnitude, a weaker underload effect is expected with negative stress ratios due to lower baseline closure levels and higher proximity of the base loading and underload minimum loads, as also discussed in the introduction with literature Refs. [16,22,26].

5.1.1. Removal of load history effect

As can be observed in Fig. 11, if the underload magnitude is equal to the global yielding threshold and notch plasticity is eliminated by using a sharp initial crack, the evolution of the post-underload opening levels corresponds very precisely to that of a new, load-history-free crack. Thus, it seems that the underload is capable of effectively removing the existing loading history, which in this case consists of the plastic wake. Fig. 23(a,b) compares the plastic wake on the crack flank before and after the underload is applied. It can be seen that the plastic wake is almost completely removed by reversed plasticity occurring during the underload. Thus, it is concluded that an underload can remove the effect of loading history. Now, it is easy to understand that the evolution of σ_{op}/σ_{max} after such an event has no other option than to exactly correspond to that of a new crack, meaning that the underload can effectively reset the opening level development. In this case, the inherent shape of the σ_{op}/σ_{max} curve plays a critical part; if the development is purely monotonic, such as in the plane stress case (See, e.g., 11), the resetting causes an overall reduction in plasticity-induced crack closure and is harmful in terms of the predicted crack driving force. However, if σ_{op}/σ_{max} development is non-monotonic, such as in the axisymmetric and plane strain cases, the resetting strengthens plasticity-induced crack closure, predicting a reduction of crack driving force. Thus, in axisymmetric and plane strain conditions, which are very similar apart from the differences in global yielding threshold and defect sensitivity, the near-tip crack closure response predicts an extension of fatigue life with single underloads, provided that compressive notch plasticity effects are absent. This includes short cracks initiating from sharp initial cracks or stiff inclusions, and long cracks. Additionally, the extent of reversed plasticity in the plastic wake is dependent on, for example, the hardening behavior; it is clear that fully reversing the plastic wake with isotropic hardening requires a much higher underload magnitude. It is worth keeping in mind that in any case, far field closure is reduced by an underload, which could play a role in terms of the crack driving force. It must also be emphasized that these conclusions are only based on the simulation results, and are yet to be validated experimentally. Nevertheless, the unusual evidence of retardation after an underload in plane strain dominated cracks [10,11] might be explained by this mechanism.

5.1.2. Notch plasticity effect

Another mechanism with a substantial influence on the underload behavior in short cracks initiated at notches or notch-like defects is notch plasticity. An underload of sufficient magnitude gives rise to compressive notch plasticity, which might not be fully countered by tensile plasticity in the crack tip. Especially with the plate-like specimens with the higher stress concentration factor, compressive notch plasticity is very harmful in terms of the post-underload opening levels (see, e.g., Fig. 10). This can also shift the residual stress state in front of the crack tip to tension, as is evident from Fig. 14(c). A region of strong compressive notch plasticity, in plane strain conditions and with underload magnitude $\sigma_{UL}/\sigma_{GY} = 0.9$, is depicted in Fig. 23(c). It is not difficult to imagine the effects of such a compressive plastic zone overshadowing the crack. The crack is essentially pulled open by the deformation, causing a reduction of crack closure and compressive residual stresses. In such a case, it should be assumed that the resistance against crack propagation cannot develop as effectively as before the underload, evidenced by Fig. 10. In that case, the underload effect would not be merely a resetting of the R-curve, as assumed in Section 4.4. If the crack is initiated at cavities, holes, notches, or even soft inclusions, the saturation of the reduction of fatigue limit as a function of the number of underloads, depicted in Fig. 22, may be accelerated, or even instant.

5.1.3. Bauschinger effect

Finally, the response to high-magnitude underloads is unexpected. The underload response changes drastically when the underload magnitude surpasses the global yielding threshold, i.e., $\sigma_{UL}/\sigma_{GY} > 1.0$, as can be seen in Fig. 7; with the plate-like specimens, the post-underload opening levels are seen to decrease until $\sigma_{UL}/\sigma_{GY} = 1.0$ due to compressive notch plasticity, but this effect is overpowered once the underload

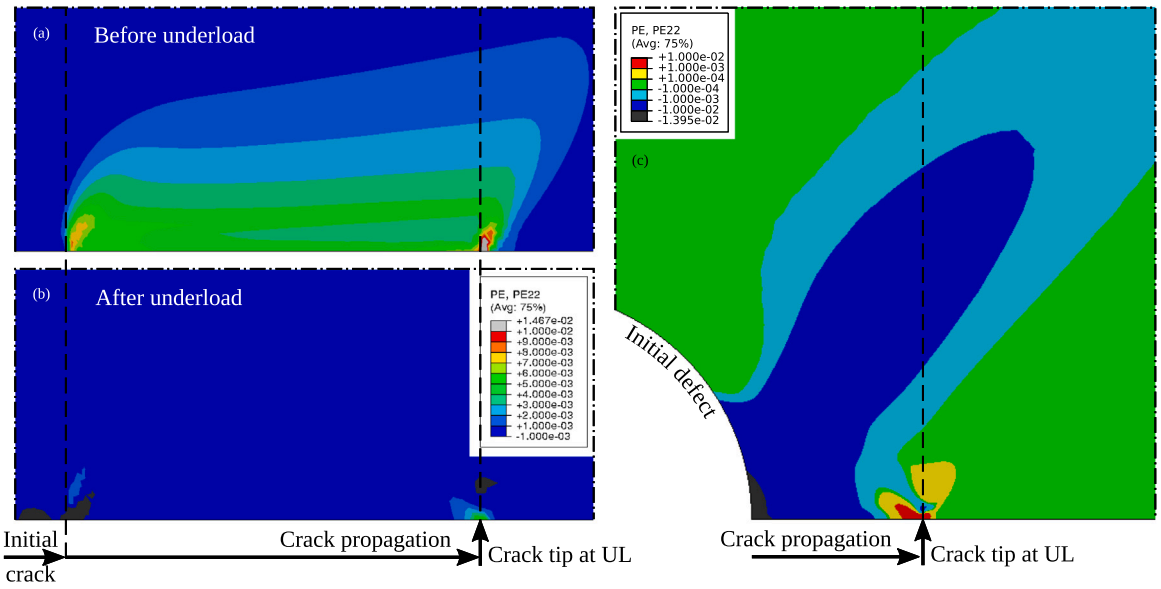

Fig. 23. Contours of the y-directional plastic strain field, (a) before and (b) after an underload with a sharp initial crack, and (c) after an underload with a round initial defect, showing compressive notch plasticity. Normalized underload magnitude is (a, b) $\sigma_{UL}/\sigma_{GY} = 1.0$ and (c) $\sigma_{UL}/\sigma_{GY} = 0.9$ (see Table 2).

magnitude is further increased. Regardless of constraint conditions and initial defect type, an underload of magnitude $\sigma_{UL}/\sigma_{GY} = 1.2$ causes an increase in plasticity-induced closure as well as a strengthening of the compressive residual stress in front of the crack tip, as shown in Figs. 7 and 15, respectively. Large underloads should therefore be beneficial in terms of fatigue life. In contrast, the underload acceleration effect is usually reported to strengthen monotonically with increasing underload magnitude [21,23,31]. However, the authors have no knowledge of experiments considering underloads well above the yield strength. Nonetheless, this phenomenon is recognized to be dependent on the occurrence of compressive plasticity in front of the crack tip resulting from the underload. If the to-be crack path is in compressive plasticity as a result of an underload, premature yielding in the crack tip will occur in tensile loading due to Bauschinger effect, promoting tensile plasticity. This is evident in Fig. 12, where a large underload increases plasticity-induced crack closure, but only with kinematic hardening. Isotropic hardening, on the other hand, only experiences the effect of the resetting of load history, resulting in a decrease of plasticity-induced closure. Thus, no higher levels of σ_{op}/σ_{max} than those of new cracks in constant amplitude loading can be expected following underloads with materials exhibiting little to no Bauschinger effect.

5.2. Reflections on prior expectations

In terms of crack closure, the textbook-esque literature overview of Table 1 was found to be very descriptive of the underload response in plane stress conditions with isotropic hardening, and also with kinematic hardening when the underload magnitude was below the global yielding threshold. In these cases the development of plasticity-induced closure was monotonic. In contrast, almost no sustained reduction of the compressive residual stress was predicted, as shown in Figs. 14, 15. This suggests that crack closure is the dominant mechanism behind the underload effect in zero–tension loading, in line with [24]. The resetting of crack closure inflicted by an underload corresponds well with a resetting of the R-curve (see Fig. 20), with both describing the reformation of a closure-free crack. Thus, solutions for the reduction of fatigue strength based on the R-curve were able to be given in Section 4.4. These results, namely Fig. 22 and Eq. (11), showed that numerous underloads were able to decrease the effective fatigue limit even to a third in certain situations. The size of the initial crack or defect was the controlling parameter for the reduction.

However, it is also clear that many of the present results were unexpected and not in line with the literature consensus. This was especially true in the cases of axisymmetric and plane strain conditions, as well as with high-magnitude underloads, where a post-underload deceleration of crack growth was consistently predicted, as evident from Fig. 17. Thus, care was taken to provide detailed physical explanations for these results. In the axisymmetric and plane strain cases, a non-monotonic development of plasticity-induced closure was predicted. However, experimental descriptions of crack closure development are mostly monotonic. For instance, the R-curve is characterized by the monotonic increase of crack propagation resistance as a function of crack length. It is worth noting, however, that most analyses consider through-plate cracks, where the monotonically developing plane stress closure may be dominant. For the present model to predict overall acceleration after a single underload, such as the plane stress curves in Fig. 17(a,b), monotonic closure development, notch plasticity or far-field closure consideration is needed. From the discrepancy to literature consensus in axisymmetric and plane strain conditions, certain deductions can be made. The fact that retardation after underloads is not observed with, for example, through-plate cracks can suggest the following:

- The monotonically developing plane stress closure on the specimen surface may be dominant in terms of crack driving force. This option is supported by the experiments already mentioned in the introduction [7], where the overload retardation phenomenon was effectively removed if the surfaces containing plane stress plasticity-induced closure were machined off after the overload was applied.
- The removal of far-field closure may be important in terms of crack driving force. This includes all forms of contact on the crack surfaces; removed is not only plasticity-induced crack closure but all closure mechanisms. The near-tip opening level may be an incomplete depiction of crack closure.
- The non-monotonic closure development predicted by the present model might not be what real cracks exhibit. A possibility is that the development of other closure mechanisms alongside plasticity-induced closure results in a monotonically developing combined influence, in line with the R-curve, for example. However, in the axisymmetric case, the authors acknowledge only one other substantial closure mechanism in addition to plasticity. The mechanism in question is roughness-induced closure; due to the internal location of the crack, oxide-induced closure is inactive.

However, direct evidence of a non-monotonic resistance curve has also been observed experimentally by Schönbauer et al. [74] with surface cracks, which are usually plane strain dominated [34]. They observed a larger ΔK_{th} value for short, defect-initiated cracks than long cracks with stress ratios exceeding approximately $R = -0.5$, suggesting a decline in the crack propagation resistance with increasing crack length. Experimental results in [75] also suggest a similar trend for a different material. This supports the predictions of non-monotonic closure development in plane strain conditions obtained in the present work, and its implications in underload scenarios. Further work is needed to answer these open questions regarding the physical nature of the underload phenomenon in fatigue. Studying of loading irregularities can reveal important details of crack closure and help to understand how it affects crack driving force also in constant amplitude loading. Future works include the experimental validation for the numerical results obtained in this paper, as well as expanding the simulation framework to more specific material models and representations of real microstructures.

6. Conclusions

The goal of this paper was to investigate the effects of single underloads to plasticity-induced crack closure in physically short cracks under different constraint conditions. Based on the results obtained, tentative guidance for fatigue design considering single and repeated underloads was able to be given. The findings are summarized below:

- A combined influence of three independent mechanisms, namely, removal of load history, compressive notch plasticity, and Bauschinger effect, was recognized to control the underload effect on plasticity-induced closure in short cracks propagating in a homogeneous continuum.
- The common experimental observation of post-underload acceleration was not able to be explained through a consideration of residual stress, but rather through crack closure, at least in zero–tension loading.
- The reversal of the existing plastic wake is considered to be the primary underload effect. Depending on the characteristic shape of closure development, the effect can be either positive or negative in terms of crack driving force.
- Short cracks emanating from cavities, holes, or soft inclusions are especially vulnerable to harmful underload effects due to compressive notch plasticity and the associated tensile residual stress.
- The level of plasticity-induced crack closure can increase heavily after an underload whose magnitude surpasses a global yielding threshold with materials exhibiting strong Bauschinger effect.
- In plane strain and axisymmetric conditions, where non-monotonic plasticity-induced closure development is predicted, single or scarce underloads may improve fatigue life. Frequent underloads, however, are always detrimental.
- A resistance curve analysis shows that fatigue limit decreases significantly and reaches a saturation value under numerous sporadic underloads, and decreases more for cracks propagating from larger defects.
- Far-field closure is removed by both over- and underloads of sufficient magnitude due to crack tip blunting. The apparent crack tip blunting associated with underloads is a result of reversed yielding in the existing crack flank.

CRediT authorship contribution statement

Kimmo Kärkkäinen: Writing – review & editing, Writing – original draft, Visualization, Software, Methodology, Investigation, Formal analysis, Data curation, Conceptualization. **Joona Vaara:** Writing – review & editing, Validation, Methodology, Investigation, Formal analysis, Conceptualization. **Miikka Väntänen:** Writing – review & editing, Conceptualization. **Mari Åman:** Writing – review & editing, Supervision. **Tero Frondelius:** Writing – review & editing, Supervision, Resources, Project administration, Funding acquisition.

Declaration of competing interest

The authors declare that they have no known competing financial interests or personal relationships that could have appeared to influence the work reported in this paper.

Data availability

Data will be made available on request.

Acknowledgments

Funded by the European Union (Grant Agreement No. 101058179; ENGINE). Views and opinions expressed are however those of the authors only and do not necessarily reflect those of the European Union or the European Health and Digital Executive Agency. Neither the European Union nor the granting authority can be held responsible for them. The authors wish to acknowledge CSC – IT Center for Science, Finland, for computational resources. The authors wish to thank the anonymous reviewers for their dedication and contribution in improving the quality of the research presented. The corresponding author wishes to thank Tauno Tönning Foundation for a personal research grant.

References

[1] Elber W. Fatigue crack closure under cyclic tension. Eng Fract Mech 1970;2(1):37–45. http://dx.doi.org/10.1016/0013-7944(70)90028-7, URL http://www.sciencedirect.com/science/article/pii/0013794470900287.
[2] Pippan R, Hohenwarter A. Fatigue crack closure: a review of the physical phenomena. Fatigue Fract Eng Mater Struct 2017;40(4):471–95. http://dx.doi.org/10.1111/ffe.12578, URL https://onlinelibrary.wiley.com/doi/abs/10.1111/ffe.12578.
[3] Wheeler OE. Spectrum loading and crack growth. J Basic Eng 1972;94(1):181–6. http://dx.doi.org/10.1115/1.3425362.
[4] Vosikovsky O, Rivard A. Growth of surface fatigue cracks in a steel plate. Int J Fatigue 1981;3(3):111–5. http://dx.doi.org/10.1016/0142-1123(81)90058-X, URL https://www.sciencedirect.com/science/article/pii/014211238190058X.
[5] Suresh S, Ritchie R. Propagation of short fatigue cracks. Int Met Rev 1984;29(1):445–75. http://dx.doi.org/10.1179/imtr.1984.29.1.445.
[6] Dexter R, Hudak S, Davidson D. Modelling and measurement of crack closure and crack growth following overloads and underloads. Eng Fract Mech 1989;33(6):855–70. http://dx.doi.org/10.1016/0013-7944(89)90101-X, URL https://www.sciencedirect.com/science/article/pii/001379448990101X.
[7] McEvily AJ, Yang Z. The nature of the two opening levels following an overload in fatigue crack growth. Metall Trans A 1990;21(10):2717–27. http://dx.doi.org/10.1007/BF02646067, URL https://link.springer.com/article/10.1007/BF02646067.
[8] Pompetzki M, Topper T, DuQuesnay D. The effect of compressive underloads and tensile overloads on fatigue damage accumulation in SAE 1045 steel. Int J Fatigue 1990;12(3):207–13. http://dx.doi.org/10.1016/0142-1123(90)90097-X, URL https://www.sciencedirect.com/science/article/pii/014211239090097X.
[9] Zhang X, Chan A, Davies G. Numerical simulation of fatigue crack growth under complex loading sequences. Eng Fract Mech 1992;42(2):305–21. http://dx.doi.org/10.1016/0013-7944(92)90221-Y, URL https://www.sciencedirect.com/science/article/pii/001379449290221Y.
[10] Carlson R, Kardomateas G. Effects of compressive load excursions on fatigue crack growth. Int J Fatigue 1994;16(2):141–6. http://dx.doi.org/10.1016/0142-1123(94)90104-X, URL https://www.sciencedirect.com/science/article/pii/014211239490104X.
[11] Buschermöhle H, Memhard D, Vormwald M. Fatigue crack growth acceleration or retardation due to compressive overload excursions. In: Fatigue, international fatigue congress, 6. Vol. 1, Oxford: Elsevier; 1996, p. 583–8, URL https://www.tib.eu/de/suchen/id/tema/TEMAW97026294457.
[12] Changqing Z, Yucheng J, Guangli Y. Effect of a single peak overload on physically short fatigue crack retardation in an axle-steel. Fatigue Fract Eng Mater Struct 1996;19(2–3):201–6. http://dx.doi.org/10.1111/j.1460-2695.1996.tb00959.x, URL https://onlinelibrary.wiley.com/doi/abs/10.1111/j.1460-2695.1996.tb00959.x.

[13] Song S-H, Lee K-R, Kim A. Analysis on short crack growth rate after single overload under cyclic bending moment. Int J Precis Eng Manuf 2001;2(3):19–26.

[14] Makabe C, Purnowidodo A, McEvily A. Effects of surface deformation and crack closure on fatigue crack propagation after overloading and underloading. Int J Fatigue 2004;26(12):1341–8. http://dx.doi.org/10.1016/j.ijfatigue.2004.03.017, URL https://www.sciencedirect.com/science/article/pii/S0142112304000970.

[15] Tvergaard V. Effect of underloads or overloads in fatigue crack growth by crack-tip blunting. Eng Fract Mech 2006;73(7):869–79. http://dx.doi.org/10.1016/j.engfracmech.2005.10.009, URL https://www.sciencedirect.com/science/article/pii/S0013794405002742.

[16] Silva F. Fatigue crack propagation after overloading and underloading at negative stress ratios. Int J Fatigue 2007;29(9):1757–71. http://dx.doi.org/10.1016/j.ijfatigue.2007.03.012, URL https://www.sciencedirect.com/science/article/pii/S0142112307001491. Fatigue Damage of Structural Materials VI.

[17] Ellyin F, Ozah F. The effect of material model in describing mechanism of plasticity-induced crack closure under variable cyclic loading. Int J Fract 2007;143(1):15–33. http://dx.doi.org/10.1007/s10704-006-9048-z, URL https://link.springer.com/article/10.1007/s10704-006-9048-z.

[18] Zhao T, Zhang J, Jiang Y. A study of fatigue crack growth of 7075-T651 aluminum alloy. Int J Fatigue 2008;30(7):1169–80. http://dx.doi.org/10.1016/j.ijfatigue.2007.09.006, URL https://www.sciencedirect.com/science/article/pii/S0142112307002708.

[19] Aguilar Espinosa A, Fellows N, Durodola J. Experimental measurement of crack opening and closure loads for 6082-T6 aluminium subjected to periodic single and block overloads and underloads. Int J Fatigue 2013;47:71–82. http://dx.doi.org/10.1016/j.ijfatigue.2012.07.010, URL https://www.sciencedirect.com/science/article/pii/S014211231200237X.

[20] Vor K, Gardin C, Sarrazin-Baudoux C, Petit J. Wake length and loading history effects on crack closure of through-thickness long and short cracks in 304L: Part II – 3D numerical simulation. Eng Fract Mech 2013;99:306–23. http://dx.doi.org/10.1016/j.engfracmech.2013.01.014, URL https://www.sciencedirect.com/science/article/pii/S0013794413000295.

[21] Zheng X, Cui H, Engler-Pinto C, Su X, Wen W. Numerical modeling of fatigue crack propagation based on the theory of critical distances: Effects of overloads and underloads. Eng Fract Mech 2014;128:91–102. http://dx.doi.org/10.1016/j.engfracmech.2014.07.006, URL https://www.sciencedirect.com/science/article/pii/S0013794414002161.

[22] Salvati E, Sui T, Zhang H, Lunt AJG, Fong KS, Song X, Korsunsky AM. Elucidating the mechanism of fatigue crack acceleration following the occurrence of an underload. Adv Energy Mater 2016;18(12):2076–87. http://dx.doi.org/10.1002/adem.201600069, URL https://onlinelibrary.wiley.com/doi/abs/10.1002/adem.201600069. arXiv:https://onlinelibrary.wiley.com/doi/pdf/10.1002/adem.201600069.

[23] Sunder R, Biakov A, Eremin A, Panin S. Synergy of crack closure, near-tip residual stress and crack-tip blunting in crack growth under periodic overloads – a fractographic study. Int J Fatigue 2016;93:18–29. http://dx.doi.org/10.1016/j.ijfatigue.2016.08.004, URL https://www.sciencedirect.com/science/article/pii/S0142112316302298.

[24] Salvati E, Zhang H, Fong KS, Song X, Korsunsky AM. Separating plasticity-induced closure and residual stress contributions to fatigue crack retardation following an overload. J Mech Phys Solids 2017;98:222–35. http://dx.doi.org/10.1016/j.jmps.2016.10.001, URL https://www.sciencedirect.com/science/article/pii/S0022509616305531.

[25] Mlikota M, Schmauder S, Božič Ž, Hummel M. Modelling of overload effects on fatigue crack initiation in case of carbon steel. Fatigue Fract Eng Mater Struct 2017;40(8):1182–90. http://dx.doi.org/10.1111/ffe.12598, URL https://onlinelibrary.wiley.com/doi/abs/10.1111/ffe.12598.

[26] Antunes FV, Paiva L, Branco R, Borrego LP. Effect of underloads on plasticity-induced crack closure: A numerical analysis. J Eng Mater Technol 2019;141(3):031008. http://dx.doi.org/10.1115/1.4042865, arXiv:https://asmedigitalcollection.asme.org/materialstechnology/article-pdf/141/3/031008/6394234/mats_141_3_031008.pdf.

[27] Vaara J, Kunnari A, Frondelius T. Literature review of fatigue assessment methods in residual stressed state. Eng Fail Anal 2020;110:104379. http://dx.doi.org/10.1016/j.engfailanal.2020.104379, URL https://www.sciencedirect.com/science/article/pii/S1350630719311483.

[28] Chen R, Zhu M-L, Xuan F-Z, Wu S-C, Fu Y-N. Near-tip strain evolution and crack closure of growing fatigue crack under a single tensile overload. Int J Fatigue 2020;134:105478. http://dx.doi.org/10.1016/j.ijfatigue.2020.105478, URL http://www.sciencedirect.com/science/article/pii/S0142112320300098.

[29] Fang X, Wang H, Li W, Liu G, Cai B. Fatigue crack growth prediction method for offshore platform based on digital twin. Ocean Eng 2022;244:110320. http://dx.doi.org/10.1016/j.oceaneng.2021.110320.

[30] Liang H, Zhan R, Wang D, Deng C, Xu X, Guo B. Effect of crack-tip deformation on fatigue crack growth: A comparative study under overload/underload conditions. Theor Appl Fract Mech 2022;118:103268. http://dx.doi.org/10.1016/j.tafmec.2022.103268, URL https://www.sciencedirect.com/science/article/pii/S0167844222000234.

[31] Liang H, Wang D, Deng C, Zhan R. Fatigue crack growth acceleration in S355 steel under a single and periodic underload. Int J Fatigue 2022;158:106744. http://dx.doi.org/10.1016/j.ijfatigue.2022.106744, URL https://www.sciencedirect.com/science/article/pii/S0142112322000251.

[32] Ritz F, Stäcker C, Beck T, Sander M. FGA formation mechanism for X10CrNiMoV12-2-2 and 34CrNiMo6 for constant and variable amplitude tests under the influence of applied mean loads. Fatigue Fract Eng Mater Struct 2018;41(7):1576–87. http://dx.doi.org/10.1111/ffe.12797, URL https://onlinelibrary.wiley.com/doi/abs/10.1111/ffe.12797.

[33] Schönbauer BM, Ghosh S, Kömi J, Frondelius T, Mayer H. Influence of small defects and nonmetallic inclusions on the high and very high cycle fatigue strength of an ultrahigh-strength steel. Fatigue Fract Eng Mater Struct 2021;44(11):2990–3007. http://dx.doi.org/10.1111/ffe.13534, URL https://onlinelibrary.wiley.com/doi/abs/10.1111/ffe.13534. arXiv:https://onlinelibrary.wiley.com/doi/pdf/10.1111/ffe.13534.

[34] Kärkkäinen K, Vaara J, Väntänen M, Niskanen I, Frondelius T. The role of plasticity-induced crack closure in the non-propagation prediction of surface defect-initiated cracks near fatigue limit. Int J Fatigue 2023;168:107462. http://dx.doi.org/10.1016/j.ijfatigue.2022.107462, URL https://www.sciencedirect.com/science/article/pii/S0142112322007125.

[35] Kärkkäinen K, Vaara J, Frondelius T. Plasticity-induced crack closure in the presence of loading irregularities in short cracks initiated at interior defects. Procedia Struct Integr 2024;57:271–9. http://dx.doi.org/10.1016/j.prostr.2024.03.029, URL https://www.sciencedirect.com/science/article/pii/S2452321624002464. Fatigue Design 2023 (FatDes 2023).

[36] Fleck NA. Acta metall. Vol. 33, 1985, p. 13339.

[37] McClung RC, Thacker BH, Roy S. Finite element visualization of fatigue crack closure in plane stress and plane strain. Int J Fract 1991;50(1):27–49. http://dx.doi.org/10.1007/BF00035167, URL https://link.springer.com/article/10.1007/BF00035167.

[38] Camas D, Garcia-Manrique J, Moreno B, Gonzalez-Herrera A. Numerical modelling of three-dimensional fatigue crack closure: Mesh refinement. Int J Fatigue 2018;113:193–203. http://dx.doi.org/10.1016/j.ijfatigue.2018.03.035, URL http://www.sciencedirect.com/science/article/pii/S0142112318301270.

[39] Zaiken E, Ritchie R. On the role of compression overloads in influencing crack closure and the threshold condition for fatigue crack growth in 7150 aluminum alloy. Eng Fract Mech 1985;22(1):35–48. http://dx.doi.org/10.1016/0013-7944(85)90157-2, URL https://www.sciencedirect.com/science/article/pii/0013794485901572.

[40] Topper TH, Sandor BI. Effects of mean stress and prestrain on fatigue-damage summation. In: Effects of environment and complex load history on fatigue life. 1970, p. 93–104. http://dx.doi.org/10.1520/STP32038S.

[41] Antunes F, Rodrigues D. Numerical simulation of plasticity induced crack closure: Identification and discussion of parameters. Eng Fract Mech 2008;75(10):3101–20. http://dx.doi.org/10.1016/j.engfracmech.2007.12.009, URL http://www.sciencedirect.com/science/article/pii/S0013794407004432.

[42] Jaeger JC, Cook NG, Zimmerman R. Fundamentals of rock mechanics. John Wiley & Sons; 2007.

[43] Davis T, Healy D, Bubeck A, Walker R. Stress concentrations around voids in three dimensions: The roots of failure. J Struct Geol 2017;102:193–207. http://dx.doi.org/10.1016/j.jsg.2017.07.013, URL https://www.sciencedirect.com/science/article/pii/S0191814117301542.

[44] Zerbst U, Madia M, Klinger C, Bettge D, Murakami Y. Defects as a root cause of fatigue failure of metallic components. I: Basic aspects. Eng Fail Anal 2019;97:777–92. http://dx.doi.org/10.1016/j.engfailanal.2019.01.055, URL https://www.sciencedirect.com/science/article/pii/S1350630718307556.

[45] Murakami Y. 5 – effect of hardness HV on fatigue limits of materials containing defects, and fatigue limit prediction equations. In: Murakami Y, editor. Metal fatigue (second edition). Academic Press; 2019, p. 61–94. http://dx.doi.org/10.1016/B978-0-12-813876-2.00005-4, URL https://www.sciencedirect.com/science/article/pii/B9780128138762000054.

[46] Pavlina E, Vantyne C. Correlation of yield strength and tensile strength with hardness for steels. J Mater Eng Perform 2008;17:888–93. http://dx.doi.org/10.1007/s11665-008-9225-5, URL https://link.springer.com/article/10.1007/s11665-008-9225-5.

[47] Murakami Y. 6 – effects of nonmetallic inclusions on fatigue strength. In: Murakami Y, editor. Metal fatigue (second edition). Academic Press; 2019, p. 95–150. http://dx.doi.org/10.1016/B978-0-12-813876-2.00006-6, URL https://www.sciencedirect.com/science/article/pii/B9780128138762000066.

[48] Murakami Y, Endo M. Effects of defects, inclusions and inhomogeneities on fatigue strength. Int J Fatigue 1994;16(3):163–82. http://dx.doi.org/10.1016/0142-1123(94)90001-9, URL https://www.sciencedirect.com/science/article/abs/pii/0142112394900019.

[49] Murakami Y, Beretta S. Small defects and inhomogeneities in fatigue strength: experiments, models and statistical implications. Extremes 1999;2(2):123–47. http://dx.doi.org/10.1023/A:1009976418553, URL https://link.springer.com/article/10.1023/A:1009976418553.

[50] Roychowdhury S, Dodds RH. A numerical investigation of 3-D small-scale yielding fatigue crack growth. Eng Fract Mech 2003;70(17):2363–83. http://dx.doi.org/10.1016/S0013-7944(03)00003-1, URL https://www.sciencedirect.com/science/article/pii/S0013794403000031.

[51] Solanki K, Daniewicz S, Newman J. Finite element modeling of plasticity-induced crack closure with emphasis on geometry and mesh refinement effects. Eng Fract Mech 2003;70(12):1475–89. http://dx.doi.org/10.1016/S0013-7944(02)00168-6, URL http://www.sciencedirect.com/science/article/pii/S0013794402001686.

[52] Oplt T, Šebík M, Berto F, Náhlík L, Pokorný P, Hutař P. Strategy of plasticity induced crack closure numerical evaluation. Theor Appl Fract Mech 2019;102:59–69. http://dx.doi.org/10.1016/j.tafmec.2019.04.004, URL https://www.sciencedirect.com/science/article/pii/S0167844218305536.

[53] McClung R, Sehitoglu H. On the finite element analysis of fatigue crack closure—1. basic modeling issues. Eng Fract Mech 1989;33(2):237–52. http://dx.doi.org/10.1016/0013-7944(89)90027-1, URL http://www.sciencedirect.com/science/article/pii/0013794489900271.

[54] Rice J. Mechanics of crack tip deformation and extension by fatigue. ASTM STP 1967;415:247–311. http://dx.doi.org/10.1520/STP47234S, URL https://www.astm.org/stp47234s.html.

[55] Singh KD, Parry MR, Sinclair I. Some issues on finite element modelling of plasticity induced crack closure due to constant amplitude loading. Int J Fatigue 2008;30(10):1898–920. http://dx.doi.org/10.1016/j.ijfatigue.2008.01.013, URL https://www.sciencedirect.com/science/article/pii/S0142112308000224.

[56] Jiang Y, Feng M, Ding F. A reexamination of plasticity-induced crack closure in fatigue crack propagation. Int J Plast 2005;21(9):1720–40. http://dx.doi.org/10.1016/j.ijplas.2004.11.005, URL http://www.sciencedirect.com/science/article/pii/S0749641904001627.

[57] Antunes FV, Borrego LFP, Costa JD, Ferreira JM. A numerical study of fatigue crack closure induced by plasticity. Fatigue Fract Eng Mater Struct 2004;27(9):825–35. http://dx.doi.org/10.1111/j.1460-2695.2004.00738.x, URL https://onlinelibrary.wiley.com/doi/abs/10.1111/j.1460-2695.2004.00738.x.

[58] Fleck N. Finite element analysis of plasticity-induced crack closure under plane strain conditions. Eng Fract Mech 1986;25(4):441–9. http://dx.doi.org/10.1016/0013-7944(86)90258-4, URL https://www.sciencedirect.com/science/article/pii/0013794486902584.

[59] Garcia-Manrique J, Camas D, Parrón-Rubio M, Gonzalez-Herrera A. Corrections in numerical methodology to evaluate plasticity induced crack closure along the thickness. Theor Appl Fract Mech 2018;97:215–23. http://dx.doi.org/10.1016/j.tafmec.2018.08.004, URL https://www.sciencedirect.com/science/article/pii/S0167844218302635.

[60] Singh KD, Khan IA. Numerical modelling of plane strain plasticity induced crack closure effects for bimaterial interfacial cracks. Int J Fatigue 2015;77:28–40. http://dx.doi.org/10.1016/j.ijfatigue.2015.03.001, URL https://www.sciencedirect.com/science/article/pii/S0142112315000584.

[61] Solanki K, Daniewicz S, Newman J. A new methodology for computing crack opening values from finite element analyses. Eng Fract Mech 2004;71(7):1165–75. http://dx.doi.org/10.1016/S0013-7944(03)00113-9, URL https://www.sciencedirect.com/science/article/pii/S0013794403001139.

[62] Camas D, Garcia-Manrique J, Antunes FV, Gonzalez-Herrera A. Numerical analysis of the influence of crack growth scheme on plasticity induced crack closure results. In: Correia JA, De Jesus AM, Fernandes AA, Calçada R, editors. Mechanical fatigue of metals. Cham: Springer International Publishing; 2019, p. 155–60. http://dx.doi.org/10.1007/978-3-030-13980-3_20, URL https://link.springer.com/chapter/10.1007/978-3-030-13980-3_20.

[63] Lee HJ, Song JH. Finite-element analysis of fatigue crack closure under plane strain conditions: stabilization behaviour and mesh size effect. Fatigue Fract Eng Mater Struct 2005;28(3):333–42. http://dx.doi.org/10.1111/j.1460-2695.2005.00881.x, URL https://onlinelibrary.wiley.com/doi/abs/10.1111/j.1460-2695.2005.00881.x.

[64] de Matos P, Nowell D. On the accurate assessment of crack opening and closing stresses in plasticity-induced fatigue crack closure problems. Eng Fract Mech 2007;74(10):1579–601. http://dx.doi.org/10.1016/j.engfracmech.2006.09.007, URL https://www.sciencedirect.com/science/article/pii/S0013794406003638.

[65] Kurihara M, Katoh A, Kawahara M. Effects of stress ratio and step loading on fatigue crack propagation rate. In: Elsevier applied science, current research on fatigue cracks. 1987, p. 247–65.

[66] American Society for Testing and Materials (ASTM). ASTM E647: standard test method for measurement of fatigue crack growth rates. In: Annual book of ASTM standards. Vol. 03.01, West Conshohocken, Pa, USA: American Society for Testing and Materials (ASTM); 1999, p. 591–630.

[67] Correia J, De Jesus A, Moreira P, Tavares P. Crack closure effects on fatigue crack propagation rates: Application of a proposed theoretical model. Adv Mater Sci Eng 2016;2016:3026745. http://dx.doi.org/10.1155/2016/3026745.

[68] Riemelmoser FO, Pippan R. Crack closure: A concept of fatigue crack growth under examination. Fatigue Fract Eng Mater Struct 1997;20(11):1529–40. http://dx.doi.org/10.1111/j.1460-2695.1997.tb01508.x, URL https://onlinelibrary.wiley.com/doi/abs/10.1111/j.1460-2695.1997.tb01508.x. arXiv:https://onlinelibrary.wiley.com/doi/pdf/10.1111/j.1460-2695.1997.tb01508.x.

[69] Maierhofer J, Pippan R, Gänser H-P. Modified NASGRO equation for physically short cracks. Int J Fatigue 2014;59:200–7. http://dx.doi.org/10.1016/j.ijfatigue.2013.08.019, URL https://www.sciencedirect.com/science/article/pii/S014211231300234X.

[70] Maierhofer J, Simunek D, Gänser H-P, Pippan R. Oxide induced crack closure in the near threshold regime: The effect of oxide debris release. Int J Fatigue 2018;117:21–6. http://dx.doi.org/10.1016/j.ijfatigue.2018.07.021, URL http://www.sciencedirect.com/science/article/pii/S0142112318303062.

[71] Maierhofer J, Kolitsch S, Pippan R, Gänser H-P, Madia M, Zerbst U. The cyclic R-curve – determination, problems, limitations and application. Eng Fract Mech 2018;198:45–64. http://dx.doi.org/10.1016/j.engfracmech.2017.09.032, URL https://www.sciencedirect.com/science/article/pii/S0013794417304046. Fracture mechanics-based determination of the fatigue strength of weldments.

[72] Zerbst U, Madia M, Vormwald M, Beier H. Fatigue strength and fracture mechanics – a general perspective. Eng Fract Mech 2018;198:2–23. http://dx.doi.org/10.1016/j.engfracmech.2017.04.030, URL https://www.sciencedirect.com/science/article/pii/S0013794417303041. Fracture mechanics-based determination of the fatigue strength of weldments.

[73] Zerbst U, Madia M. Fracture mechanics based assessment of the fatigue strength: approach for the determination of the initial crack size. Fatigue Fract Eng Mater Struct 2015;38(9):1066–75. http://dx.doi.org/10.1111/ffe.12288, URL https://onlinelibrary.wiley.com/doi/abs/10.1111/ffe.12288. arXiv:https://onlinelibrary.wiley.com/doi/pdf/10.1111/ffe.12288.

[74] Schönbauer BM, Mayer H. Effect of small defects on the fatigue strength of martensitic stainless steels. Int J Fatigue 2019;127:362–75. http://dx.doi.org/10.1016/j.ijfatigue.2019.06.021, URL https://www.sciencedirect.com/science/article/pii/S0142112319302531.

[75] Yamabe J, Kobayashi M. Effect of hardness and stress ratio on threshold stress intensity factor ranges for small cracks and long cracks in spheroidal cast irons. J Solid Mech Mater Eng 2007;1(5):667–78. http://dx.doi.org/10.1299/jmmp.1.667.